The effects of technological voids on the hydro-mechanical behaviour of compacted bentonite-sand mixture

Qiong Wang, Anh Minh A.M. Tang, Yu-Jun Cui, Pierre Delage,
Jean-Dominique Barnichon, Wei-Min Ye

1 The effects of technological voids on the hydro-mechanical

2 behaviour of compacted bentonite-sand mixture

3

4 Qiong Wang[1], Anh Minh Tang[1], Yu-Jun Cui[1,3], Pierre Delage[1], Jean-Dominique
5 Barnichon [2], Wei-Min Ye[3]

6

7 *[1] Ecole des Ponts ParisTech, Navier/CERMES[1], France*
8 *[2] Institut de Radioprotection et de Sûreté Nucléaire (IRSN), France*
9 *3. Tongji University, China*

10
11
12
13
14
15
16 **<u>Corresponding author:</u>**
17 Prof. Yu-Jun CUI
18 *Ecole des Ponts ParisTech*
19 6-8 av. Blaise Pascal, Cité Descartes, Champs-sur-Marne
20 77455 MARNE LA VALLEE
21 France
22
23 Telephone : +33 1 64 15 35 50
24 Fax : +33 1 64 15 35 62
25 E-mail : yujun.cui@enpc.fr

---

[1] Centre d'Enseignement et de Recherches en Mécanique des Sols

26   **Abstract**

27   Compacted bentonite-based materials are often used as buffer materials in radioactive
28   waste disposal. A good understanding of their hydro-mechanical behaviour is essential
29   to ensure the disposal safety. In this study, a mixture of MX80 bentonite and sand was
30   characterized in the laboratory in terms of water retention property, swelling pressure,
31   compressibility and hydraulic conductivity. The effects of the technological voids or
32   the voids inside the soil were investigated. The technological voids are referred to as
33   the macro-pores related to different interfaces involving the buffer material, whereas
34   the voids inside the soil is referred to as the common macro-pores within the
35   compacted bentonite/sand mixture. The results obtained show that at high suctions,
36   the amount of water absorbed in the soil depends solely on suction, whereas at low
37   suctions it depends on both suction and bentonite void ratio. There is a unique
38   relationship between the swelling pressure and the bentonite void ratio, regardless of
39   the sample nature (homogeneous or not) and sand fraction. However, at the same
40   bentonite void ratio, a higher hydraulic conductivity was obtained on the samples with
41   technological voids. The effect of sand fraction was evidenced in the mechanical yield
42   behaviour: at the same bentonite void ratio, the bentonite-sand mixture yielded at a
43   higher pre-consolidation stress.
44
45   **Keywords:** Bentonite-sand mixture; Technological voids effects; Water retention
46   property; Swelling pressure; Hydraulic conductivity; Compressibility.
47
48

49   **1 INTRODUCTION**

50   Most designs of deep geological repository for high level radioactive wastes (HLW)
51   are based on the multi-barrier concept with isolation of the waste from the
52   environment. The multi-barrier concept includes the natural geological barrier (host
53   rock), engineered barriers made up of compacted sand-bentonite mixtures (placed
54   around waste containers or used as buffer and sealing elements) and metal canister.
55   Compacted bentonite-based materials are relevant materials for this purpose thanks to
56   their low permeability, high swelling and high radionuclide retardation capacities
57   (Pusch, 1979; Yong et al., 1986; Villar and Lloret, 2008; Komine and Watanabe, 2010;
58   Cui et al., 2011).

59   Engineered barriers are often made up of compacted bricks. When bricks are placed
60   around waste canisters or to form sealing buffers, the so-called technological voids
61   either between the bricks themselves or between bricks, canisters and the host rock
62   are unavoidable. As an example, 10 mm thick gaps between bentonite blocks and
63   canister and 25 thick mm gaps between the bentonite blocks and the host rock have
64   been considered in the basic design of Finland (Juvankoski, 2010). These
65   technological voids appeared to be equal to 6.6 % of the volume of the gallery in the

FEBEX mock-up test (Martin et al., 2006). Fractures that appear in the excavation damaged zone within the host rock in the near field constitute additional voids. In the French concept, the volume of the bentonite/rock gaps is estimated at 9 % of the volume of the gallery by the French waste management agency (ANDRA 2005). This value reaches 14 % in the SEALEX in-situ test carried out in the Tournemire Underground Research Laboratory (URL) run by IRSN (Institut de radioprotection et de sûreté nucléaire, the French expert national organisation in nuclear safety) in South-West of France (Barnichon and Deleruyelle, 2009).

Once placed in the galleries, engineered barriers are progressively hydrated by pore water infiltrating from the host-rock. This water infiltration is strongly dependent on the initial state of the compacted material (water content, suction and density, e.g. Cui et al. 2008). Indeed, it has been shown that water transfer in unsaturated swelling compacted bentonites or sand bentonite mixtures is strongly dependent on the imposed boundary conditions in terms of volume change. As shown in Yahia-Aissa et al. (2001), Cui et al. (2008) and Ye et al. (2009), the degree of swelling allowed significantly affects the amount of infiltrated water, with much water absorbed when swelling is allowed and a minimum amount of water absorbed when swelling is prevented. Volume change conditions also appeared to have, through microstructure changes, significant influence on the hydraulic conductivity.

In this regard, the degree of swelling allowed by the technological voids described above has a significant influence on the hydro-mechanical behaviour of the compacted bentonite and their effects need to be better understood. Swelling results in a decrease in dry density that may lead to a degradation of the hydro-mechanical performance of engineered barriers (Komine et al., 2009, Komine, 2010). As a result, the safety function expected in the design may no longer be properly ensured. Therefore, a better understanding of the effects of the technological voids is essential in assessing the overall performance of the repository.

In this study, a series of tests was performed on a compacted bentonite-sand mixture samples, aiming at investigating the effects of technological voids on their hydro-mechanical behaviour. Temperature effects were not considered and tests were carried out at constant ambient temperature (20±1°C). Given that the paper deals with the hydration of engineered barriers in the repository, neither the drying process nor hysteresis effects were considered.

Firstly, the water retention curve was determined under both free swell and restrained swell conditions; secondly, the effects of a pre-existing technological void on both the swelling pressure and hydraulic conductivity were investigated; finally, the compressibility at different void ratios was studied by means of suction-controlled oedometer tests. An overall analysis of the effects of voids on the hydro-mechanical response of the engineered barrier was finally performed.

2 MATERIALS AND METHODS

2.1 Materials and sample preparation

A commercial MX80 Na-bentonite from Wyoming, USA was used. The bentonite powder was provided with an initial water content of 12.2% and was stocked in a hermetic container to maintain the water content constant, in a room at 20±1°C. All tests were performed at this temperature.

This MX80 Na-bentonite is characterised by a high montmorillonite content (80%), a liquid limit of 575%, a plastic limit of 53% and a unit mass of the solid particles of 2.77 Mg/m^3. The cation exchange capacity (CEC) is 76 meq/100g (83 % of Na). The grain size distribution (Figure 1) determined using a hydrometer (French standard AFNOR NF P94-057) on deflocculated clay shows that the clay fraction (< 2 µm) is 84%. The X-Ray diffractometer diagram of the clay fraction presented in Figure 2 shows a peak at 12.5 Å, typical of montmorillonite (this peak shifted from 12.5 to 16.9 Å when treated with glycol and to 9.5 Å when dried). These data are comparable with that provided by Montes-H et al., (2003).

The sand used in the mixture was a quartz sand from the region of Eure and Loire, France, that passed through a 2 mm sieve. Figure 1 shows the sand grain size distribution curve determined by dry sieving (AFNOR NF P94-056). The curve is characterized by a uniformity coefficient C_u of 1.60 and a D_{50} close to 0.6 mm. The unit mass of the sand grains is 2.65 Mg/m^3.

A water having the same chemical composition as the pore water of the Callovo-oxfordian claystone from the ANDRA URL in Bure (France), called synthetic water, was used in the experiments. The corresponding chemical components (see Table 1) were mixed with distilled water in a magnetic stirrer until full dissolution.

The grain size distribution of the bentonite powder obtained by "dry" sieving is also presented in Figure 1, showing a well graded distribution around a mean diameter slightly larger than 1 mm. This curve is close to that of sand. The powder was carefully mixed with dry sand (70% bentonite - 30% sand in mass) giving a water content of 8.5% for the mixture. Prior to compaction, the mixture powder was put into a hermetic container connected to a vapor circulation system (see Figure 3) containing free water (100% relative humidity), so as to reach a target water content of 11%. The samples were weighed every two hours until the target water content was attained (after around two days).

A given quantity of mixture was then placed into a rigid ring (35 or 38 mm diameter) and statically compacted using an axial press at a constant displacement rate of 0.05 mm/min to different target dry densities (values given in the following section). Once the target dry density reached, the displacement shaft was fixed for more than

143 15 h to attain axial stress stabilization (defined by changes in axial stress as low as
144 0.05 MPa/h). This procedure minimized the sample rebound during unloading.

145 The results from Mercury intrusion porosimetry (MIP) tests on the bentonite/sand
146 mixtures compacted to dry densities $\rho_d = 1.67$ and 1.97 Mg/m^3 and freeze dried are
147 shown in Figure 4. A typical bimodal porosity (e.g. Ahmed et al. 1974, Delage et al.
148 1996, Romero et al. 1999) was observed in both samples, defining intra-aggregate
149 pores (micro-pores) with a mean size of 0.02 μm and inter-aggregate pores
150 (macro-pores) that depend on the dry density and range from 10 μm (for $\rho_d = 1.67$
151 Mg/m^3) to 50 μm ($\rho_d = 1.97$ Mg/m^3). As shown by Delage and Graham (1995) from
152 the data of Sridharan et al. (1971), this confirms that compaction only affects the
153 largest inter-aggregate pores while intra-aggregate pores remain unaffected (see also
154 Lloret and Villar, 2007). In compacted bentonites, it has been shown that a further
155 smaller sized pore population (ranging between 0.2 and 2 nm) corresponding to the
156 intra-particle (interlayer) pores within the aggregates and not detectable by the MIP
157 had to be also considered (Delage et al., 2006; Lloret and Villar, 2007).

158 **2.2 Experimental methods**

159 2.2.1 Water retention test

160 The water retention curve (WRC) of the bentonite/sand mixture was determined under
161 both free swell and restrained swell conditions by using both the vapour equilibrium
162 technique (s > 4.2 MPa) and osmotic technique (s < 4.2 MPa) for suction control.
163 Three identical samples were used in parallel and the final water content calculated
164 corresponds to the mean value. To apply suction by the vapour equilibrium technique
165 under free swell conditions the as-compacted sample (35 mm diameter and 5 mm
166 height) was placed into a desiccator containing a saturated salt solution at bottom. The
167 sample mass was regularly measured to monitor the water content variation over time.
168 In a standard fashion, equilibrium was considered reached when the mass stabilized.
169 To apply the osmotic technique (Delage et al. 1998; Delage and Cui, 2008a and
170 2008b), the sample was wrapped by a cylinder-shaped semi-permeable membrane and
171 placed in a PEG 20 000 solution at a concentration corresponding to the required
172 suction. The water content at equilibrium under each suction was determined by
173 weighing.

174 Following Yahia-Aissa et al. (2001), the determination of the water retention curve
175 under prevented swell conditions (constant volume conditions) was carried out on
176 samples of 50 mm in diameter and 5 mm in height, placed into a specially designed
177 rigid stainless steel cell allowing vapour exchanges through two metal porous disks
178 put on both sides. To apply the osmotic technique, the semi-permeable membrane was
179 placed between the porous stone and the soil sample (Figure 5a); all was then
180 sandwiched between two perforated discs and immersed into a PEG solution at the
181 required concentration. Water infiltrated into the soil through the porous stone and the

182 semi-permeable membrane until the target suction was reached. To apply suction with
183 the vapour equilibrium technique, the sample sandwiched between two porous stones
184 was installed between two external plates with valves (Figure 5b) that were connected
185 to a suction control system using the vapour equilibrium technique. The water content
186 at equilibrium under each suction was determined by weighing.

187 All the tests performed and the solutions used for suction control (Delage et al., 1998;
188 Ye et al., 2009) are presented in Table 2. Samples were statically compacted at a dry
189 density of 1.67 Mg/m^3, corresponding to the final dry density adopted in the in situ
190 experiment at the Tournemire URL.

191 2.2.2 Hydration test with technological void (SP 01 - 04)

192 The effect of technological void on the swelling behaviour of the compacted
193 sand-bentonite mixture was investigated using the device shown in Figure 6. In this
194 system, a sample is placed inside an oedometer cell placed into a rigid frame
195 comprising a load transducer that allows the measurement of vertical stress during
196 hydration. The small vertical strain due to the deformability of the set-up is measured
197 by a digital micrometer.

198 A technological void of 14% of the total cell volume that corresponds to the situation
199 of the SEALEX in situ test at the Tournemire URL was set by choosing an initial
200 diameter of the compacted sample smaller than that of the hydration cell. With a ring
201 diameter of 38 mm, the annular technological void selected (14% of the total cell
202 volume representing 17% of the initial sample volume) corresponded to a sample
203 diameter of 35.13 mm.

204 The sample was hydrated by injecting synthetic water under constant pressure
205 (0.1 MPa) through a porous disk in contact with the bottom face while the top face
206 was put in contact with another porous stone so as to allowed free expulsion of either
207 air or water (see Figure 6). The small water pressure (0.1 MPa) was adopted to avoid
208 any effect on axial pressure measurement. Changes in axial stress, displacement and
209 injected water volume over time were monitored. Once the axial stress stabilized
210 (after more than 35 h , see Figure 9), water injection under 0.1 MPa was continued for
211 24 h more in order to determine the hydraulic conductivity under permanent flow
212 condition. Indeed, a linear relationship between flux and time was observed,
213 confirming the observation of Dixon et al. (1992) about the validity of Darcy's law for
214 saturated compacted bentonites.

215 Four tests with the same technological void of 14% (SP01 - SP04) were conducted on
216 samples with the same initial water content of 11% and various initial dry densities
217 obtained by changing the compaction pressure (between 65 and 85 MPa, giving rise to
218 dry densities comprised between 1.93 and 1.98 Mg/m^3, see Table 3). An initial axial
219 stress of 0.5 MPa was applied on the specimen before hydration to ensure good
220 contact and satisfactory load measurement (see Figure 6). When water injection

221 started, the piston was fixed and the build-up of axial stress was monitored by the load
222 transducer.

223 2.2.3 Suction controlled oedometer test (SO-01 SO-04)

224 Controlled suction oedometer compression tests were carried out on samples of 10
225 mm in height and 38 mm in diameter by circulating vapour at controlled relative
226 humidity at the base of the sample as shown in Figure 7 (tests SO-02/04). A high
227 pressure oedometer frame was used so as to apply vertical stresses as high as 50 MPa
228 (Marcial et al., 2002). Zero suction was applied by circulating pure water. Vertical
229 strain was monitored using a digital micrometer (accuracy ±0.001 mm).

230 Prior to compression, samples were hydrated under a low vertical stress of 0.1 MPa
231 by applying a suction lower than the initial as-compacted value (estimated at 65 MPa
232 from the water retention curve in Figure 8 at $w = 11\%$).

233 As seen in Table 4, the testing program includes 3 standard tests (SO-02 to 04) carried
234 out on 38 mm diameter samples with an initial dry density of 1.67 Mg/m^3 under
235 controlled suctions of 4.2, 12.6 and 38 MPa, respectively. Stabilisation of swelling
236 under the imposed suctions and a vertical stress of 0.1 MPa were waited for prior to
237 compression.

238 The configuration of test SO-01 ($\rho_{di} = 1.97$ Mg/m^3, internal diameter of 35.13 mm), is
239 similar to that described in Figure 6, with an annular void between the sample and
240 ring corresponding to a 14% technological void. In this test, the sample was flooded
241 with synthetic water, imposing zero suction through the liquid phase. The higher
242 1.97 Mg/m^3 density was chosen so as to correspond to the previous value of 1.67
243 Mg/m^3 once the technological void clogged by the lateral sample swelling. Obviously,
244 even though that the global density of sample SO-01 was equal to that of samples
245 SO-02/04 after swelling, the density of sample SO-01 should not be homogeneous
246 and should follow a rather axisymetrical distribution, with lower values in the zone of
247 former technological void clogged by soil swelling.

248

3 EXPERIMENTAL RESULTS

3.1 Water retention curves

251 Figure 8 presents the wetting path of the water retention curves (WRCs) obtained
252 under both free swell and restrained swell conditions. For suctions higher than 9 MPa,
253 the two curves are very similar while a significant difference can be identified in the
254 range of suction below 9 MPa. When suction reached 0.01 MPa, the water content
255 under free swell condition is 246.0%, a much higher value than that under restrained
256 swell condition (25.4%). This confirms that the prevented swelling condition

257 significantly affects the retention property only in the range of low suctions
258 (Yahia-Aissa et al. 2001, Cui et al. 2008, Ye et al. 2009).

259 The WRCs of samples of pure MX80 bentonite compacted to 1.7 Mg/m^3 dry unit
260 mass under both free swell and constant volume conditions determined by Marcial
261 (2003) are also presented in Figure 8. In the higher suction range (s > 9 MPa), all data
262 fall on the same curve, regardless of the imposed condition (swelling allowed or
263 constant volume) and type and density of material (bentonite-sand mixture at
264 1.67 Mg/m^3 or pure bentonite at 1.7 Mg/m^3). By contrast, at lower suctions
265 (s < 9MPa), the water content of the mixture under free swell condition is lower than
266 that of the pure bentonite at the same suction value.

3.2 Effects of the technological void (tests SP01-SP04)

268 Figure 9 presents the results of the four tests (SP01-SP04) carried out to investigate
269 the effect of technological void on the swelling pressure during water injection under
270 a constant pressure of 0.1 MPa. As seen in Photo 1, some water escaping from the top
271 of the cell was observed at the beginning of water injection during the initial increase
272 of vertical stress (Figure 9). This phase of 25-30 min duration corresponded to the
273 circulation of water in the annular gap between the sample and the ring. After this
274 period, the gap was obviously filled by hydrated bentonite with no more outflow
275 observed. After about 35 h, the vertical stress reached stabilization with final values of
276 2.07, 2.77, 2.44, and 3.06 MPa for tests SP01 (ρ_{di} = 1.93 Mg/m^3), SP02 (ρ_{di} = 1.96
277 Mg/m^3), SP03 (ρ_{di} = 1.96 Mg/m^3) and SP04 (ρ_{di} = 1.98 Mg/m^3), respectively. Note
278 that even though the piston was fixed (Figure 6), small volume changes (vertical
279 displacements between 10 and 90 µm) were recorded by the displacement transducer
280 because of the deformability of the system.

3.3 Controlled suction compression tests (SO-01, SO-02, SO-03 and SO-04)

282 The changes in vertical strain with time during suction imposition for tests SO-01,
283 SO-02, SO-03 and SO-04 are presented in Figure 10. In a standard fashion, higher
284 vertical strain rates were observed at smaller suctions with final strains of 1.2% (e =
285 0.69), 5.4% (e = 0.73), 6.8% (e = 0.75) and 18.0% (e = 0.97) obtained for suctions of
286 38 MPa, 12.6 MPa, 4.2 MPa and 0 MPa, respectively.

287 The significantly faster hydration observed in test SO-01 (in which liquid water was
288 used imposing a zero suction) was mainly due to the technological void that allowed
289 water circulation around the sample. This first phase was comparable with that of tests
290 SP-02/04 presented in Figure 9.

291 Figure 11 depicts the final void ratios obtained versus the imposed suctions in a
292 semi-logarithmic plot. The points are reasonably located along a line and the
293 following relationship can be derived:

294 $$e = -0.048\ln(s) + 0.848 \qquad\qquad \text{(Eq.1)}$$

295 where e is the void ratio at equilibrium and s is suction in MPa.

296 Once equilibrated at the desired suction, samples were submitted to controlled-suction
297 compression. The compression curves are presented in Figure 12 in a diagram giving
298 the changes in void ratio e with respect to vertical net stress $(\sigma_v - u_a)$ in which u_a is
299 the air pressure, equal to the atmospheric pressure. Given the significant concerns
300 about the validity of effective stress in unsaturated soils, it was preferred to use the
301 independent variables approach involving the vertical net stress $(\sigma_v - u_a)$ and suction
302 $(s = u_w - u_a)$, (Coleman 1962, Fredlund and Morgenstern, 1977, Gens 1996).

303 Initial void ratios were very different because of the significant dependence of initial
304 swelling with respect to the suction imposed. Also, the sample SO-01 was not a
305 homogeneous one, as commented above.

306 Each sample exhibited a slightly S-shaped compression curve. In a standard fashion,
307 the compression curves are characterized by an initial linear branch with a low
308 compressibility (pseudo-elastic domain) followed by a second branch with a higher
309 compressibility (plastic domain) and a slight upward curvature at higher stresses.

310 As suggested by other authors (Keller et al., 2004; Tang et al., 2009), the points at
311 high stresses were not used for determining the compression coefficient (C_c) and the
312 yield stress (σ_y) delimitating the pseudo-elastic zone and the plastic one. Figure 13
313 shows the changes in yield stress with respect to suction. Also plotted in this Figure
314 are the data obtained by Marcial (2003) on pure bentonite samples. Figure 13
315 confirms that suction decrease significant reduce the yield stress for both the mixture
316 and pure bentonite samples. There is a linear relationship between yield stress and
317 suction, and moreover, both curves are reasonably parallel. At a same suction, smaller
318 yield stresses are observed for the mixture.

319 As also observed by Marcial (2003), the change in compression coefficient with
320 respect to suction appeared to be non monotonic (Figure 14) with a decrease when
321 suction was reduced from 38 MPa and 12.6 MPa, followed by an increase when
322 suction was below 12.6 MPa. Comparison between pure bentonite and sand-bentonite
323 mixture shows that at any suction, the latter appears to be more compressible with a
324 larger compression coefficient.

325 **3.4 Hydraulic conductivity measurements**

326 The hydraulic conductivity of hydrated samples with initial technological void (tests
327 SP2-SP4) was measured under constant head when applying the 0.1 MPa water
328 pressure by recording the volume of injected water by means of a Pressure/Volume
329 controller (no data were available for test SP01 due to a technical problem with the
330 Pressure/Volume controller). The determination of hydraulic conductivity was done
331 over the last 24 h once swelling stabilised. The hydraulic conductivity was also
332 determined indirectly based on the consolidation curves during different compression
333 stages of test SO-01 (see Figure 12) using Casagrande's method. As mentioned

334 before, the sample density was not homogeneous in those samples. Therefore, a non
335 uniform hydraulic conductivity can be expected for each sample. The measured
336 values correspond to the global hydraulic conductivity.

337 The changes in hydraulic conductivity with respect to dry density obtained from both
338 methods are presented in Figure 15 and compared with constant head permeability
339 measurements obtained by Gatabin et al. (2008) on homogeneous samples at similar
340 densities. The data obtained for the heterogeneous samples with both methods are in
341 good agreement. In a standard fashion, the hydraulic conductivity decreases with
342 density increase following a slope comparable to that obtained by Gatabin et al.
343 (2008). An in-depth examination shows that the samples tested here exhibit higher
344 hydraulic conductivity than that by Gatabin et al. (2008), with a difference of one
345 order of magnitude. This difference is suspected to be due to a preferential water flow
346 in the looser zone (initial technological voids) around the samples.

347

348 ## 4 INTERPRETATION AND DISCUSSION

349 In order to further analyse the effects of the technological void, various constitutive
350 parameters of the compacted mixture are now defined (see Figure 16), such as for
351 instance the bentonite void ratio (e_b). It is supposed that the volume of bentonite (V_b)
352 in the mixture is equal to the difference between the total volume (V) and the volume
353 of sand (V_s). V_b is equal to the sum of the bentonite particle volume (V_{bs}) and the
354 volume of void, namely intra-void volume (V_i). The parameter e_b consists of two parts
355 (Eq.2), the intra-bentonite void ratio inside the soil (e_{bi}) and the void ratio
356 corresponding to the technological void (e_{tech}). Eq.3 and Eq. 4 define these two voids,
357 respectively.

358
$$e_b = e_{bi} + e_{tech} \qquad \text{(Eq.2)}$$

359
$$e_{bi} = \frac{V_i}{V_{bs}} \qquad \text{(Eq.3)}$$

360
$$e_{tech} = \frac{V_{tech}}{V_{bs}} \qquad \text{(Eq.4)}$$

361 where V_{tech} is the volume of technological void. The value of e_{bi} can be deduced from
362 the initial dry unit mass of the mixture (ρ_{dm}) using Eq.5 and Eq.6.

363
$$e_{bi} = \frac{G_{sb}\rho_w}{\rho_{db}} - 1 \qquad \text{(Eq.5)}$$

364
$$\rho_{db} = \frac{(B/100)\rho_m G_{ss}\rho_w}{G_{ss}\rho_w(1 + w_m/100) - \rho_m(1 - B/100)} \qquad \text{(Eq.6)}$$

365 where ρ_w is the water unit mass, G_{sb} is the specific gravity of bentonite, ρ_{db} is the

366 initial dry unit mass of bentonite in the mixture, which was calculated using Eq.6
367 (Dixon et al., 1985; Lee et al., 1999; Agus and Schanz, 2008; Wang et al., 2012), ρ_m is
368 the unit mass of the mixture, B (%) is the bentonite content (in dry mass) in the
369 mixture, G_{ss} is the specific gravity of sand, w_m is the water content of the mixture. In
370 this study the decrease of water unit mass (ρ_w) during hydration (e.g. Skipper et al.,
371 1991; Villar and Lloret, 2004) was not considered and the value was assumed to be
372 constant (1.0 Mg/m^3), $B = 70\%$, $G_{ss} = 2.65$.

373 To analyse the water retention property under free swell condition, a parameter
374 namely water volume ratio (e_w) defined as the ratio of water volume (V_w) to the
375 bentonite volume (V_{bs}) is also adopted (Romero et al., 2011). This parameter can be
376 deduced from the water content of the mixture (w_m) using the following equation:

$$e_w = \frac{w_m \mathrm{G}_{sb}}{B}$$

377 (Eq.7)

378 In the following, the two parameters e_b and e_w are used to analyze all experimental
379 results obtained in order to evidence the effects of voids on the water retention
380 capacity, the swelling pressure, the compressibility and the hydraulic conductivity.

381 **4.1 Water retention curves**

382 Figure 17a shows the changes in water volume ratio e_w of both the mixture and the
383 pure bentonite with respect to suction under free swell condition. Unlike in the water
384 content/suction plot (Figure 8), Figure 17a shows an excellent agreement with Marcial
385 (2003)'s data on pure bentonite, with a unique relationship between e_w and suction
386 along the wetting path with swelling. It confirms that water was only adsorbed in the
387 bentonite (volume V_{bs}) and that the lower water content observed in the mixture at
388 same suction (Figure 8) is related to the lower volume of bentonite in the mixture.

389 The results from the hydration tests on pure compacted bentonites under restrained
390 swell condition with different void ratios (Marcial, 2003; Tang and Cui, 2010; Villar,
391 2005) are also presented in Figure 17. A phenomenon similar to that observed in the
392 water content/suction plane (Figure 8) can be identified: in the range of low suctions
393 (<9 MPa for the MX80 bentonite), the water retention property of bentonite depends
394 strongly on the confining conditions; conversely, all curves become almost the same
395 in the range of high suctions (as also observed by Agus 2005 and Agus et al. 2010) As
396 suggested by Cui et al. (2002, 2008) and Ye et al. (2009), this confirms that the
397 exfoliation of clay particles from the aggregates into inter-aggregate pores caused by
398 hydration is moderate and can be accommodated at high suctions. By contrast, at
399 lower suctions, available pores become completely full by hydrated clay particles and
400 no more water can be adsorbed. This is not the case when swelling is allowed with
401 much more water adsorbed. Figure 17b is a zoom of Figure 17a at small water volume
402 ratios (between 0 and 1.5). The difference observed in the curves at constant volume

403 is due to differences in bentonite dry density ρ_{db}. When the full saturation is
404 approached, samples with a higher bentonite void ratio (lower dry density) logically
405 absorb more water for a given suction.

4.2 Hydration test with technological void

407 The values of vertical stress measured on heterogeneous samples at the end of the
408 hydration tests on samples with technological voids (SP 01-04) are presented in
409 Figure 18 with respect to the bentonite void ratio. Note that the bentontie void ratios
410 for tests SP 01-04 were determined by taken into account the system deformation
411 mentioned above (i.e. vertical displacements between 10 and 90 µm). The data of
412 swelling stresses measured in homogeneous samples under the same conditions of
413 constant volume by other authors are also plotted for comparison (MX80 70/30
414 bentonite/sand mixture from Karnland et al., 2008 and pure MX80 bentonite from
415 Börgesson et al., 1996; Dixon et al., 1996; Karnland et al., 2008; Komine et al., 2009).

416 All data remarkably agree, providing a unique relationship between the vertical
417 pressure and the bentonite void ratio, regardless of the sample nature (homogeneous
418 or not). The correspondence with data from Karnland (pure bentonite and 70/30
419 bentonite sand mixture) at bentonite void ratio close to 1 is particularly good. The
420 following expression can be deduced for the relationship between the axial stress (σ_s
421 in MPa) and the bentonite void ratio e_b for the material studied here:

$$\sigma_s = 2.250 e_b^{-1.149} \qquad \text{(Eq.8)}$$

423 This good correspondence between the response in swelling stress of homogeneous
424 samples and that in axial stress of a hydrated heterogeneous sample indeed confirms
425 that the stress at equilibrium is not affected by the heterogeneity of the samples. The
426 pressure (σ_s in MPa) only depends on the global bentonite void ratio (e_b), regardless
427 of the technological void and of the presence of sand.

428 In other words, during the hydration under constant global volume and in spite of their
429 significant difference in form and dimension, the technological voids play the same
430 role as the macro-pores of the homogeneous compacted bentonite in terms of filling
431 voids by particle exfoliation, as commented above. The global final bentonite void
432 ratio (or density) appears to be a relevant parameter allowing predicting the final axial
433 stress obtained.

4.3 Compressibility

435 The interpretation of the compressibility data was based on the well known features of
436 the aggregate microstructure of compacted soils that have been recalled above,
437 showing in particular that the compression at constant water content of unsaturated
438 compacted soils initially occurs by the collapse of large inter-aggregate pores full of
439 air with little effect on the aggregates themselves. As a consequence, it was observed

440   that the changes in suction during compression at constant water content are
441   negligible, since suction changes are governed by intra-aggregate clay water
442   interactions that are little affected during compression (Li, 1995; Gens et al., 1995;
443   Tarantino and De Col, 2008).

444   The compression curves of the homogeneous samples in Figure 12 (SP2 to 4) are
445   further interpreted by an approximated estimation of the changes in degree of
446   saturation during compression. This estimation is based on the assumption that the
447   order of magnitude of the initial water contents of the samples hydrated from the
448   initial as-compacted suction (65 MPa) at given suctions (38, 12.6 and 4.2 MPa) prior
449   to compression can be obtained from the wetting path of the water retention curve in
450   Figure 17. Based on this assumption, the water contents after hydration were
451   determined, equal to 12.8, 16.8 and 18.6 % for suctions of 38, 12.6 and 4.2 MPa,
452   respectively. The corresponding degrees of saturation are 52, 63 and 68%,
453   respectively.

454   The application of suctions as high as 4.2, 12.6 and 38 MPa generated a moderate
455   swelling of the samples, with void ratio increasing from the initial value of 0.64 to
456   0.75 at 4.2 MPa suction. In terms of microstructure, the changes corresponds to a
457   moderate swelling of the aggregates within a structure still significantly desaturated
458   with a maximum degrees of saturation of 68% at 4.2 MPa suction, indicating that the
459   inter-aggregates pores remained full of air. During compression, the water content that
460   was controlled within the aggregates did not suffer from any significant changes and
461   the changes in degree of saturation could be estimated, as shown in Figure 19. The
462   data show how the degree of saturation increase with increased stress and provide an
463   estimation of the stress values at which saturation was reached (9, 14 and 27 MPa at
464    $s = 4.2$, 12.6 and 38 MPa respectively). Once reported on the compression curves of
465   Figure 12, we can observe that these stress values are located close to the inflection
466   points observed on the curves, indicating that these points correspond to the saturation
467   of the samples. In other words, the change in slope of the curves corresponds to the
468   transition between two physical mechanisms, namely from the collapse of dry
469   inter-aggregate pores to the expulsion of inter-aggregate adsorbed water. This is in
470   agreement with the observation by Kochmanová and Tanaka (2011).

471   When the yield stress (σ_{v0}) in Figure 13 is plotted versus the corresponding bentonite
472   void ratio (e_b) at the yield point (Figure 20), it appears that for both the mixture and
473   pure bentonite, the yield stress increases sharply with decreasing bentonite void ratio.
474   However, the curve of the mixture lies in the right of the pure bentonite's one,
475   evidencing the role of sand in the compression behaviour. It can be concluded from
476   Figure 20 that at the same bentonite void ratio, the mixture yields at a higher
477   pre-consolidation stress.

478   **4.4 Hydraulic conductivity**

479   The values of global hydraulic conductivities presented in Figure 15 showed possible

480   preferential flow pathway in the case of heterogeneous samples with initial
481   technological voids. This observation can be made also in Figure 21 in which the data
482   of Figure 15 are re-plotted versus the bentonite void ratio and compared to other data
483   of the pure MX80 bentonite (Karnland et al., 2008; Dixon et al., 1996) and of the
484   70/30 bentonite-sand mixture (Gatabin et al., 2008). The good agreement observed
485   also confirms a negligible effect of sand on the hydraulic conductivity.

486   Note that the looser zone corresponding to the initial technological void is a weak
487   zone with poorer mechanical resistance, at least on the short term. The question of the
488   possible further changes that could occur on the long term is opened, given that some
489   observations already showed that ageing effects are significant in compacted
490   bentonite, both at microscopic scale (Delage et al. 2006) and macroscopic scale
491   (Stroes-Gascoyne, 2010), showing a tendency towards density homogenisation.
492   Further studies are needed to investigate the long term change in hydraulic
493   conductivity of samples with initial technological voids.
494

495   ## 5 CONCLUSION

496   The effects of voids on the hydro-mechanical properties of a compacted
497   bentonite-sand mixture were studied. Water retention test, hydration test, suction
498   controlled oedometer test and hydraulic test were performed on samples with different
499   voids including the technological void and the void inside the soil. By introducing the
500   parameters as bentonite void ratio and water volume ratio, the effects of voids on the
501   water retention property, the swelling pressure, the compressibility and the hydraulic
502   conductivity were analyzed.

503   Under different conditions (free swell and restrained swell), different water retention
504   properties were observed depending on the suction value: at high suctions, the relation
505   between the water volume ratio and the suction is unique, independent of the test
506   conditions, indicating that the relatively limited exfoliated clay particles are mainly
507   accommodated by the macro-pore of the soil. On the contrary, in the range of low
508   suctions, the macro-pores available for accommodating exfoliated particles becomes
509   limited in the case of restrained swell condition, explaining why less water is
510   adsorbed in this case.

511   There is a unique relationship between the axial stress (for samples with technological
512   void) or swelling pressure (constant volume condition) and the bentonite void ratio,
513   regardless of the sample nature (homogeneous or not) and presence of sand,
514   suggesting that the technological voids play the same role as the macro-pores of the
515   homogeneous compacted bentonite. It also reveals that the swelling mechanisms of
516   bentonite-sand mixture are the same as that of pure bentonite.

517   The change in slope of the compression curves corresponds to the transition between
518   two physical mechanisms, namely from the collapse of dry inter-aggregate pores to

519   the expulsion of inter-aggregate adsorbed water.

520   At the same bentonite void ratio, bentonite/sand mixture yields at a higher
521   pre-consolidation stress, evidencing the effect of sand on the compression behaviour.

522   Similar relationship between hydraulic conductivity and bentonite void ratio was
523   observed for the bentonite-sand mixture and the pure bentonite without technological
524   void; however, with the technological void in this study, the measured hydraulic
525   conductivity for the same bentonite void ratio is generally higher, indicating the
526   possible preferential flow pathway formed by the swollen soil that occupied the initial
527   technological void.

528   From a practical point of view, the relationship elaborated between the
529   hydro-mechanical behaviour with bentonite void ratio is helpful in designing the
530   buffers/sealing elements with bentonite-based materials: if the bentonite proportion
531   and the technological void are known, the specification of the buffer elements could
532   be determined using the correlations elaborated in this study, according to the
533   requirements in terms of swelling pressure and hydraulic conductivity. Then the water
534   retention property and compressibility of the selected material can be evaluated. It
535   should be however noted that the conclusion drawn here was based on the results of
536   the bentonite/sand mixture with 70% of MX80 bentonite. Further experimental studies
537   on other proportions and other bentonites are needed to generalise it.

ACKNOWLEDGEMENTS

REFERENCES

544

545   AFNOR, 1992. AFNOR NF P94-057, Soils: investingation and testing. Granulometric
546   analysis. Hydrometer method. Association Francaise de Normalisation. France.
547   AFNOR, 1996. AFNOR NF P94-056, Soils: investigation and testing. Granulometric analysis.
548   Dry sieving method after washing. Association Francaise de Normalisation. France.
549   Agus, S.S, 2005. An Experimental study on hydro-mechanical characteristics of compacted
550   bentonite-sand mixtures. PhD thesis. Weimar.
551   Agus, S.S., and Schanz, T., 2008. A method for predicting swelling pressure of compacted
552   bentonites. Acta Geotechnica, 3(2), 125-137.
553   Agus, S.S., and Schanz, T., and Fredlund, D.G., 2010. Measurements of suction versus water
554   content for bentonite-sand mixtures. Can. Geotech. J, 47, 583-594.
555   Ahmed. S., Lovell. C.W. & Diamond. S. 1974. Pore sizes and strength of compacted clay.
556   ASCE Journal of the Geotechnical Engineering Division 100, 407-425.

557   Andra, 2005. Référentiel des matériaux d'un stockage de déchets à haute activité et à vie
558   longue - Tome 4: Les matériaux à base d'argilites excavées et remaniées. Rapport Andra
559   N° CRPASCM040015B.
560   Barnichon, J.D. and Deleruyelle, F., 2009. Sealing Experiments at the Tournemire URL.
561   EUROSAFE.
562   Börgesson, L., Karnland, O., Johannesson L.E., 1996. Modelling of the physical behaviour of
563   clay barriers close to water saturation.pdf: Modelling of the physical behaviour of clay
564   barriers close to water saturation.Engineering Geology 41, 127-144.
565   Coleman, J.D. 1962. Stress-Strain relations for partially saturated soils. Géotechnique 12 (4),
566   348-350.
567   Cui, Y.J., Loiseau, C. and Delage, P., 2002. Microstructure changes of a confined swelling soil
568   due to suction controlled hydration. Unsaturated soils: proceedings of the Third
569   International Conference on Unsaturated Soils, 10-13, March 2002, Recife, Brazil,
570   593-598.
571   Cui, Y.J., Tang, A.M., Loiseau, C., Delage, P., 2008. Determining the unsaturated hydraulic
572   conductivity of a compacted sand-bentonite mixture under constant-volume and
573   free-swell conditions. Physics and Chemistry of the Earth, Parts A/B/C, 33 (Supplement
574   1), S462 - S471.
575   Cui, Y.J., Tang, A.M., Qian, L.X., Ye, W.M., Chen, B., 2011. Thermal-mechanical behavior of
576   compacted GMZ Bentonite. Soils and Foundations, Vol. 51, No. 6, 1065-1074.
577   Delage P. & Graham J. 1995. The mechanical behaviour of unsaturated soils. Proceedings of
578   the 1st International Conference on Unsaturated soils, Vol. 3, 1223-1256, Paris, E.E.
579   Alonso and P. Delage eds, Balkema.
580   Delage, P., Audiguier, M., Cui, Y.J. & Howat, M.D. 1996. Microstructure of a compacted silt.
581   Canadian Geotechnical Journal, 33 (1), 150-158.
582   Delage,P., Howat, M.D., Cui., Y.J., 1998. The relationship between suction and swelling
583   properties in a heavily compacted unsaturated clay. Engineering Geology, 50(1-2),
584   31-48.
585   Delage, P., Marcial, D., Cui, Y.J., Ruiz, X., 2006. Ageing effects in a compacted bentonite: a
586   microstructure approach. Géotechnique 56 (5), 291-304.
587   Delage, P. and Cui, Y.J. 2008a. An evaluation of the osmotic method of controlling suction.
588   Journal of Geomechanics and Geoengineering 3 (1), 1-11.
589   Delage, P. and Cui, Y.J. 2008b. A novel filtration system for polyethylene glycol solutions
590   used in the osmotic method of controlling suction. Canadian Geotechnical Journal 45,
591   421-424.
592   Dixon, D.A., Gray, M.N. and Thomas, A.W., 1985. A study of the compaction properties of
593   potential clay-sand buffer mixtures for use in nuclear fuel waste disposal. Engineering
594   Geology, 21, 247-255.
595   Dixon, D.A., Gray, M.N., Hnatiw, D., 1992. Critical gradients and pressures in dense swelling
596   clays. Canadian Geotechnical Journal 29 (6), 1113-1119.
597   Dixon, D.A., Gray, M.N., Graham, J., 1996. Swelling and hydraulic properties of bentonites
598   from Japan, Canada and USA. In Proceedings of the second International Congress on
599   Environmental Geotechnics, Osaka, Japan, 5-8.
600   Fredlund D.G. & Morgenstern N.R. 1977. Stress state variables for unsaturated soils. ASCE J.

601 Geotech. Eng. Div. GT5, 103, 447-466.

602 Gatabin, C., Touze, G., Imbert, C., Guillot, W., Billaud, P., 2008. ESDRED Project, Module
603 1-Selection and THM characterization of the buffer material. In International conference
604 underground disposal unit design&emplacement processes for a deep geological
605 repository, 16-18 June, Prague.

606 Gens, A., Alonso, E.E., Suriol, J., Lloret, A., 1995. Effect of structure on the volumetric
607 behaviour of a compacted soil. In: Alonso, Delage (Eds.), Proc. 1st Int. Conf. on
608 Unsaturated Soils, Paris, vol. 1. Balkema, Rotterdam, 83-88.

609 Gens, A., 1996. Constitutive modelling : Application to compacted soils . Proc. 1st Int. Conf
610 on Unsaturated Soils UNSAT' 95, Vol. 3, 1179-1200, Paris.

611 Juvankoski, M., 2010. Description of basic design for buffer (working report 2009-131).
612 Technical report, EURAJOKI , FINLAND.

613 Karnland, O., Nilsson, U., Weber, H., and Wersin, P., 2008. Sealing ability of Wyoming
614 bentonite pellets foreseen as buffer material-Laboratory results. Physics and Chemistry
615 of the Earth, Parts A/B/C, 33, S472-S475.

616 Keller, T., Arvidsson, J., Dawidowski, J.B., Koolen, A.J., 2004. Soil precompression stress. II.
617 A comparison of different compaction tests and stress - displacement behaviour of the
618 soil during wheeling. Soil Till. Res. 77, 97-108.

619 Kochmanová, N., Tanaka, H., 2011. Influence of the Soil Fabric on the Mechanical Behaviour
620 of Unsaturated and Saturated Clay. Soils and Foundations, Vol. 51, No. 2, 275-286.

621 Komine, H. and Yasuhara, K. and Murakami, S. 2009. Swelling characteristics of bentonites
622 in artificial seawater. Canadian Geotechnical Journal. 46, 177-189

623 Komine, H., 2010. Predicting hydraulic conductivity of sand bentonite mixture backfill before
624 and after swelling deformation for underground disposal of radioactive wastes.
625 Engineering Geology. 114, 123-134

626 Komine, H., Watanabe, Y., 2010. The past, present and future of the geo-environment in Japan.
627 Soils and Foundations, Vol. 50 (2010) No. 6 977-982.

628 Lee, J.O., Cho, W.J. and Chun, K.S., 1999. Swelling Pressures of a Potential Buffer Material
629 for High-Level Waste Repository. Journal of the Korean Nuclear Society, 31, 139-150.

630 Li, Z.M., 1995. Compressibility and collapsibility of compacted unsaturated loessial soils. In:
631 Alonso, Delage (Eds.), Proc. 1st Int. Conf. on Unsaturated Soils, Paris, vol. 1.Balkema,
632 Rotterdam, 139-144.

633 Lloret, A.., Villar, M., 2007. Advances on the knowledge of the thermo-hydro-mechanical
634 behaviour of heavily compacted FEBEX bentonite. Physics and Chemistry of the Earth,
635 32, 701-715

636 Marcial, D., Delage, P. and Cui, Y.J. 2002. On the high stress compression of bentonites.
637 Canadian Geotechnical Journal 39, 812-820.

638 Marcial, D., 2003. Comportement hydromécanique et microstructural des matériaux de
639 barrière ouvragée, thèse ENPC.

640 Martin, P.L., Barcala, J.M., and Huertas, F., 2006. Large-scale and long-term coupled
641 thermo-hydro-mechanic experiments with bentonite: the febex mock-up test. Journal of
642 Iberian Geology, 32(2), 259-282.

643 Montes-H, G., Duplay, J., Martinez, L., and Mendoza, C. 2003. Swelling–shrinkage kinetics
644 of MX80 bentonite. Applied Clay Science, 22, 279-293.

645 Pusch, R., 1979, Highly compacted sodium bentonite for isolating rock-deposited radioactive
646   waste products. Nucl. Technol.;(United States), 45(2).

647 Romero, E., Gens, A. & Lloret, A., 1999. Water permeability, water retention and
648   microstructure of unsaturated compacted Boom clay. Engineering Geology. 54, 117-127.

649 Romero, E., Della Vecchia, G., and Jommi, C., 2011. An insight into the water retention
650   properties of compacted clayey soils. Geotechnique 61, No. 4, 313-328.

651 Skipper, N.T., Refson, K., McConnell, J.D.C., 1991. Computer simulation of interlayer water
652   in 2:1 clays. J. Chem. Phys. 94 (11), 7434-7445.

653 Sridharan, A., Altschaeffle, A. G. and Diamond, S. (1971), Pore size distribution studies,
654   Journal of the Soil Mechanics and Foundations Division, Proceedings of the ASCE, vol.
655   97, SM 5, 771-787

656 Stroes-Gascoyne, S. 2010. Microbial occurrence in bentonite-based buffer, backfill and
657   sealing materials from large-scale experiments at AECL's underground research
658   laboratory. Applied Clay Science, 47(1-2), 36-42.

659 Tang, A.M., Cui, Y.J., Eslami, J. Defossez, P., 2009. Analysing the form of the confined
660   uniaxial compression curve of various soils . Geoderma vol (148)3-4, 282-290.

661 Tang, A.M and Cui, Y.J., 2010, Effects of mineralogy on thermo-hydro-mechanical
662   parameters of MX80 bentonite, Journal of Rock Mechanics and Geotechnical
663   Engineering. 2 (1), 91-96.

664 Tarantino, S. and De Col, E., 2008. Compaction behaviour of clay. Géotechnique, vol. 58
665   (3), 199-213.

666 Villar, M.V. and Lloret. A., 2004. Influence of temperature on the hydro-mechanical
667   behaviour of a compacted bentonite. Applied Clay Science, 26(1-4), 337-350.

668 Villar, M.V., 2005, MX-80 Bentonite. Thermo-Hydro-Mechanical Characterisation Performed
669   at CIEMAT in the Context of the Prototype Project. CIEMAT Technical Report:
670   CIEMAT/DIAE/54540/2/04.

671 Villar, M.V., Lloret, A., 2008. Influence of dry density and water content on the swelling of a
672   compacted bentonite. Applied Clay Science, 39(1-2), 38-49.

673 Wang Q., Tang A.M., Cui Y.J., Delage P., Gatmiri B. 2012. Experimental study on the
674   swelling behaviour of bentonite/claystone mixture. Engineering Geology 124, 59-66.

675 Yahia-Aissa, M., Delage, P., & Cui, Y.J. 2001. Suction-water relationship in swelling clays.
676   Clay science for engineering, IS-Shizuoka International Symposium on Suction, Swelling,
677   Permeability and Structure of Clays, 65-68, Adachi & Fukue eds, Balkema.

678 Ye, W.M., Cui, Y.J., Qian, L.X., and Chen. B., 2009. An experimental study of the water
679   transfer thro ugh confined compacted gmz bentonite. Engineering Geology, 108(3-4),
680   169-176.

681 Yong, R.N., Boonsinsuk, P., and Wong, G., 1986. Formulation of backfill material for a
682   nuclear fuel waste disposal vault. Canadian Geotechnical Journal, 23(2), 216-228.

683

684

685

686

687 **List of Tables**

688

689   Table 1 Chemical composition of the synthetic water

690   Table 2 Test conditions for water retention property

691   Table 3 Specimens used for swelling pressure test

692   Table 4 Specimens used for suction controlled oedometer test

693

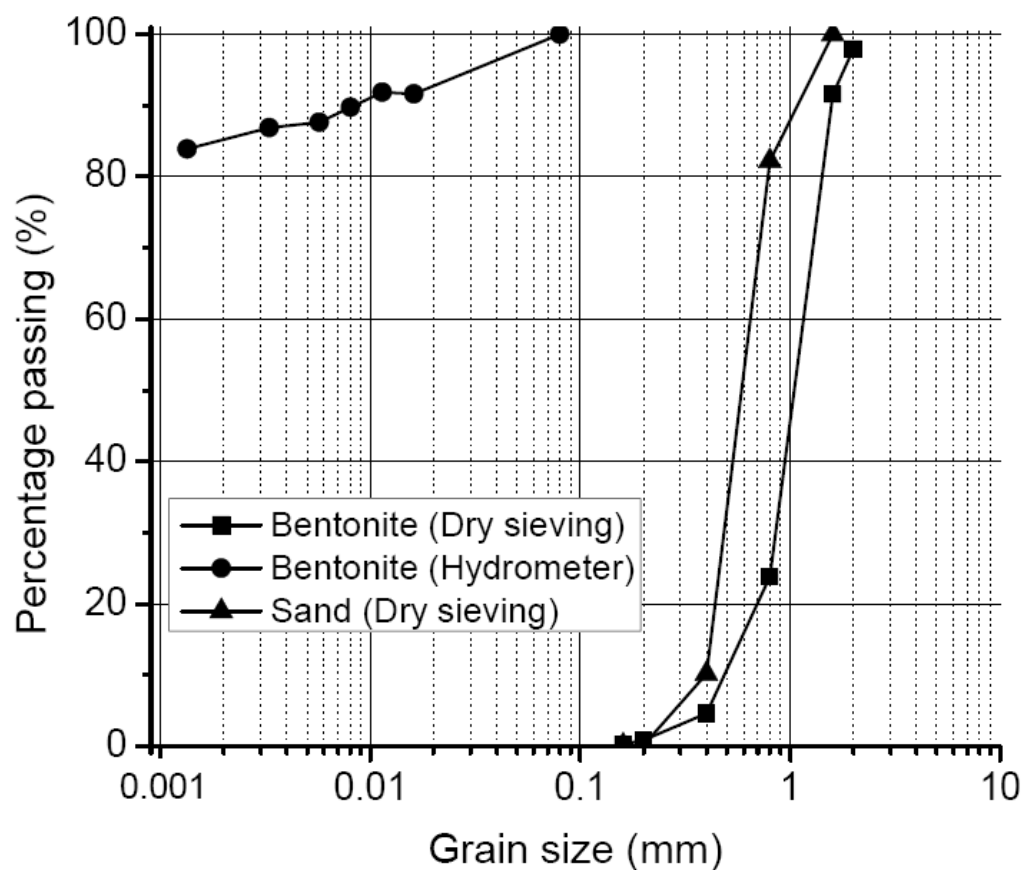694   **List of Figures**

695

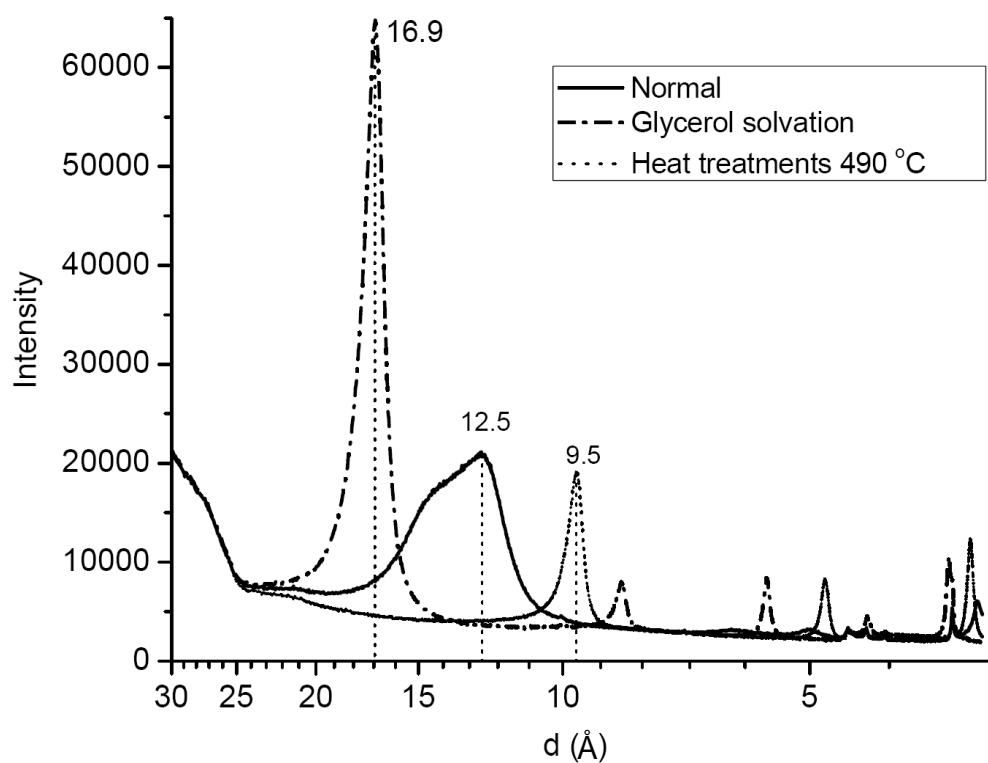696   Figure 1. Grain size distribution of the MX80 bentonite and sand

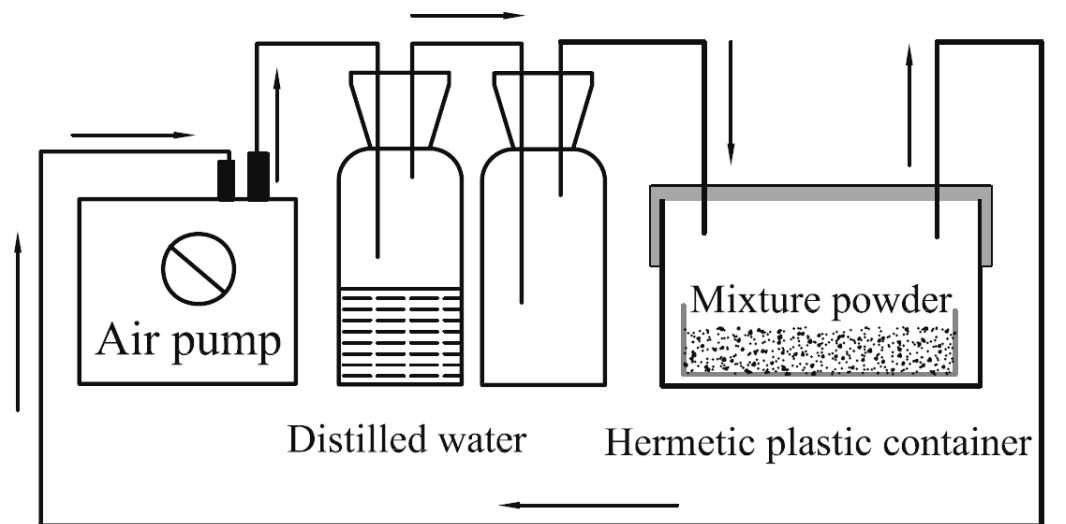697   Figure 2. X-Ray curves of the MX80 bentonite

698   Figure 3. Hermetic plastic container with a vapor circulation system for adjusting water
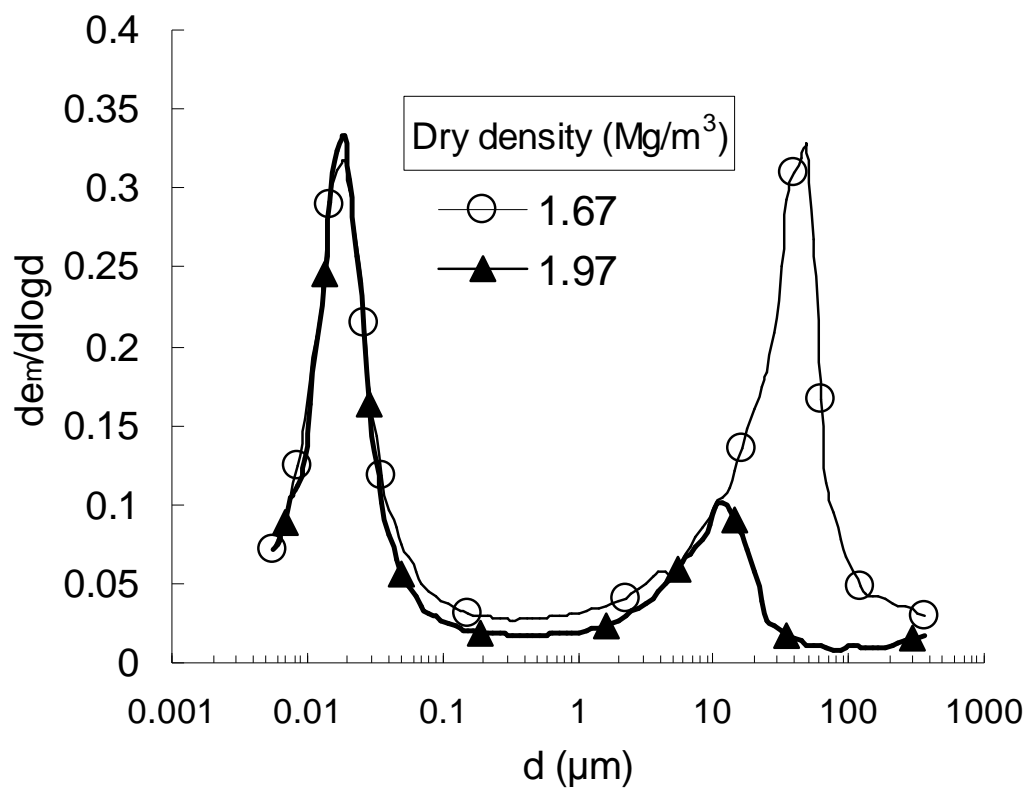699   content

700   Figure 4. Pore size distribution of bentonite/sand mixture compacted to different dry density
701   with a water content of about 11.0%

702   Figure 5. Constant volume cell for WRC determination. (a) Osmotic method; (b) Vapour
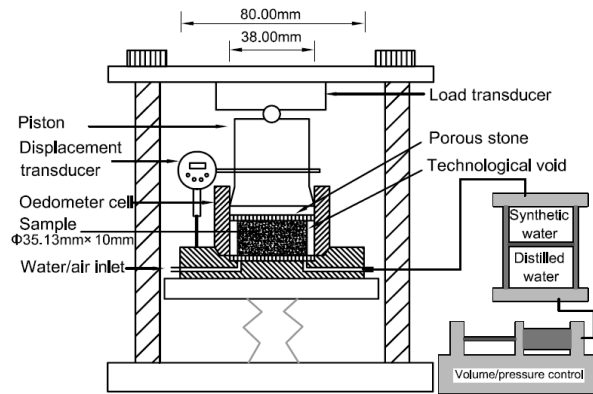703   equilibrium technique

704   Figure 6. Schematic layout of hydration test with technological void
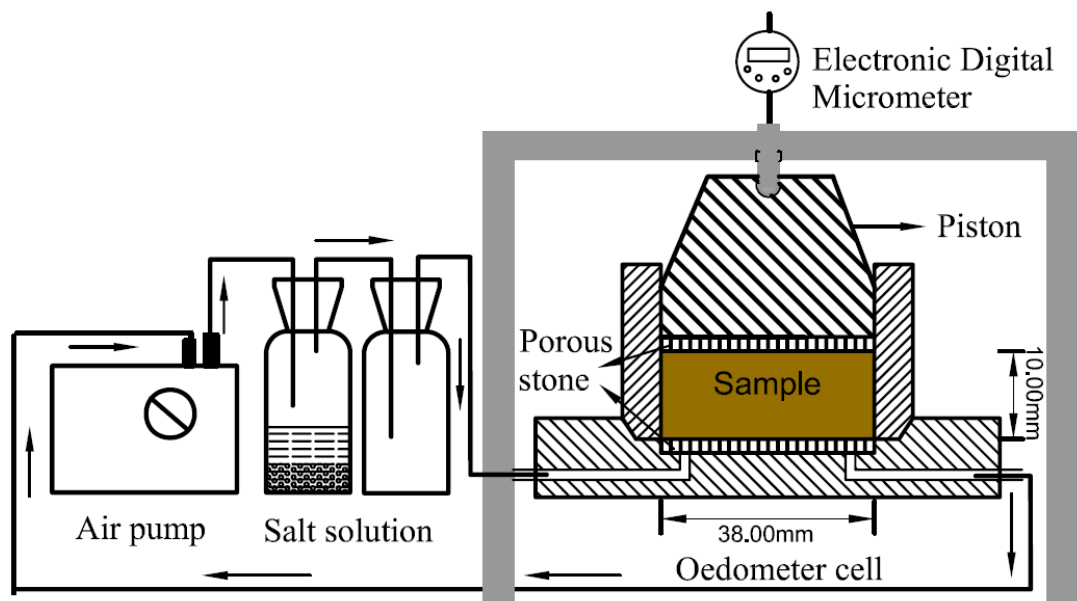
705   Figure 7. Experimental setup of suction controlled oedometer test

706   Figure 8. WRCs of bentonite-sand mixture and pure bentonite

707   Figure 9. Evolution of the axial stress for all hydration tests with technological void

708   Figure 10. Evolution of vertical strain during suction imposition

709   Figure 11. Relationship between void ratio and suction for the compacted sand bentonite
710   mixture

711   Figure 12. Void ratio of soil versus vertical net stress for different suctions

712   Figure 13. Changes in yield stress with suction

713   Figure 14. Changes in compression coefficient with suction

714   Figure 15. Hydraulic conductivity versus dry density of mixture

715   Figure 16. Composition of the bentonite/sand mixture

716   Figure 17. Water volume ratio (e_w) Versus suction. a) full range of water volume ratio; b) zoom
717   on the range of low water volume ratio

718   Figure 18. Relationship between vertical stress or axial stress and bentonite void ratio

719   Figure 19. Changes in degree of saturation during compression

720   Figure 20. Relationship between yield stress and bentonite void ratio

721   Figure 21. Hydraulic conductivity versus bentonite void ratio

722

723   **List of Photos**

724

725   Photo 1. Water outflow through the technological void.

726

727

728

729

730

731

732 Table 1. Chemical composition of the synthetic water

Components	NaHCO$_3$	Na$_2$SO$_4$	NaCl	KCl	CaCl$_2$.2H$_2$O	MgCl$_2$.6H$_2$O	SrCl$_2$.6H$_2$O
Mass (g) per Litter of solution	0.28	2.216	0.615	0.075	1.082	1.356	0.053

733

734 Table 2. Test conditions for water retention property

Suction control method		Suction (MPa)	constant volume	Free swell
	LiCl	309	_	√
	K$_2$CO$_3$	113	_	√
	Mg(NO$_3$)$_2$	82	_	√
Saturated	NaCl	38	√	√
salt solution	(NH4)$_2$SO$_4$	24.9	√	√
	ZnSO$_4$	12.6	√	√
	KNO$_3$	9.0	√	√
	K$_2$SO$_4$	4.2	√	√
Concentration	0.302	1	√	√
of PEG solution	0.095	0.1	√	√
(g PEG/g Water)	0.030	0.01	√	√

735

736 Table 3. Specimens used for swelling pressure test

Tests	Compaction Stress (MPa)	Compacted dry density (Mg/m^3)
SP01	65	1.93
SP02	70	1.96
SP03	80	1.96
SP04	85	1.98

737

738 Table 4 Specimens used for suction controlled oedometer test

Tests	ρ_{di} (Mg/m^3)	D (mm)	s (MPa)
SO-01	1.97	35.13	0
SO-02	1.67	38.00	4.2
SO-03	1.67	38.00	12.6
SO-04	1.67	38.00	38

739

740

741   Figure 1. Grain size distribution of the MX80 bentonite and sand

742

743   Figure 2. X-Ray curves of the MX80 bentonite

744

745

746   Figure 3. Hermetic plastic container with a vapor circulation system for adjusting water
747   content

748

749

750   Figure 4. Pore size distribution of bentonite/sand mixture compacted to different dry density
751   with a water content of about 11.0%

752

753

754

755

756

757

758

759

760

761

762

763

(a)

764

765

766

767
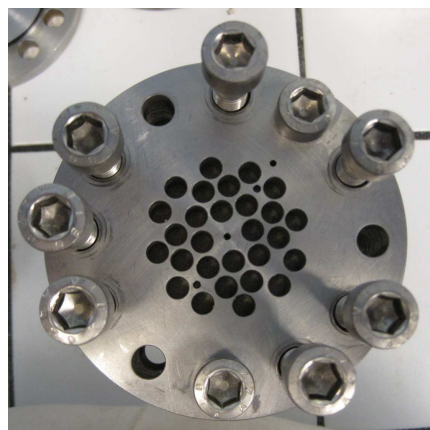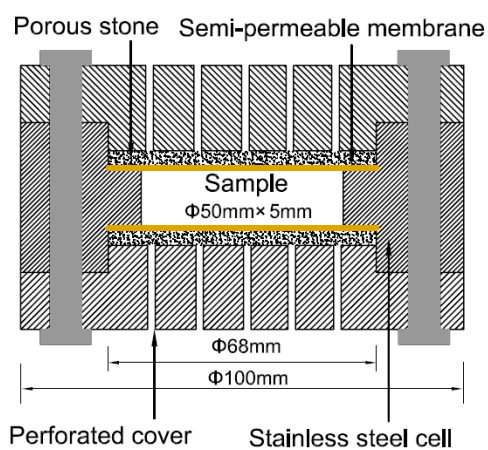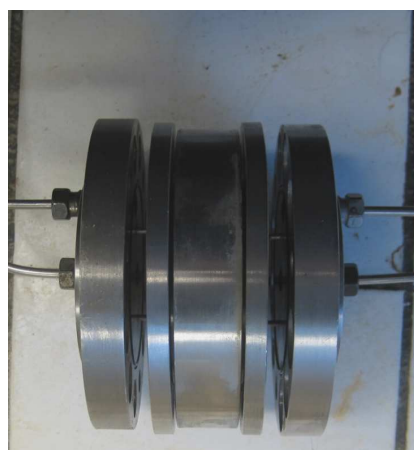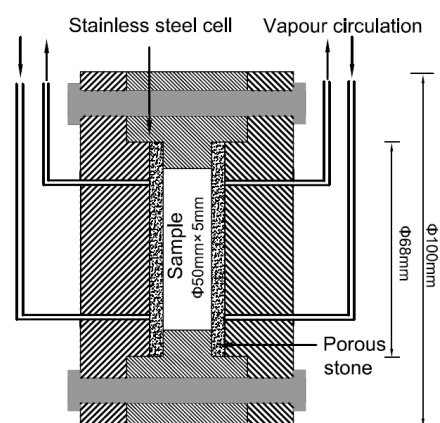
(b)

Figure 5. Constant volume cell for WRC determination. (a) Osmotic method; (b) Vapour equilibrium technique

768

769

770

771   Figure 6. Schematic layout of hydration test with technological void

772

773   Figure 7. Experimental setup of suction controlled oedometer test

774
775
776
777
778
779
780
781
782
783
784
785
786

787

788   Figure 8. WRCs of bentonite-sand mixture and pure bentonite

789

790

791

792

793

794

795
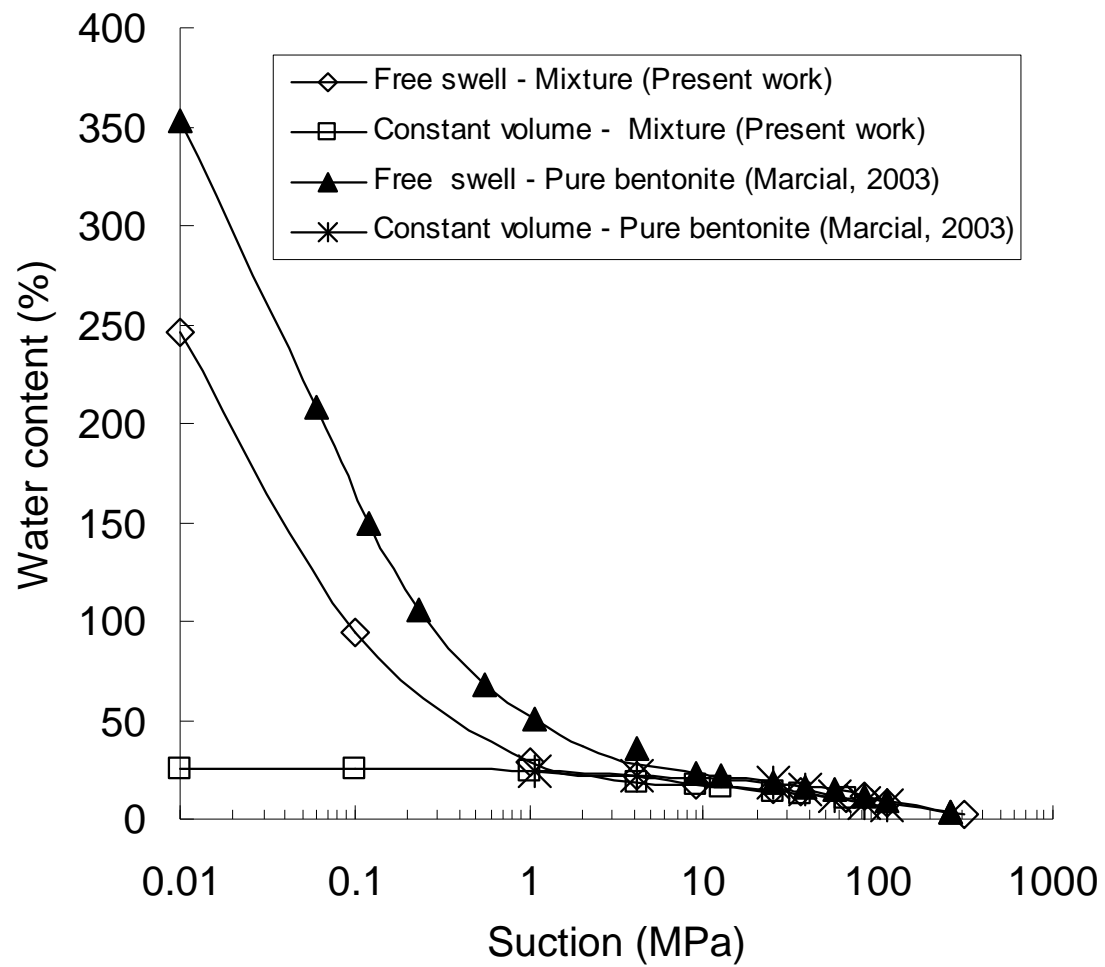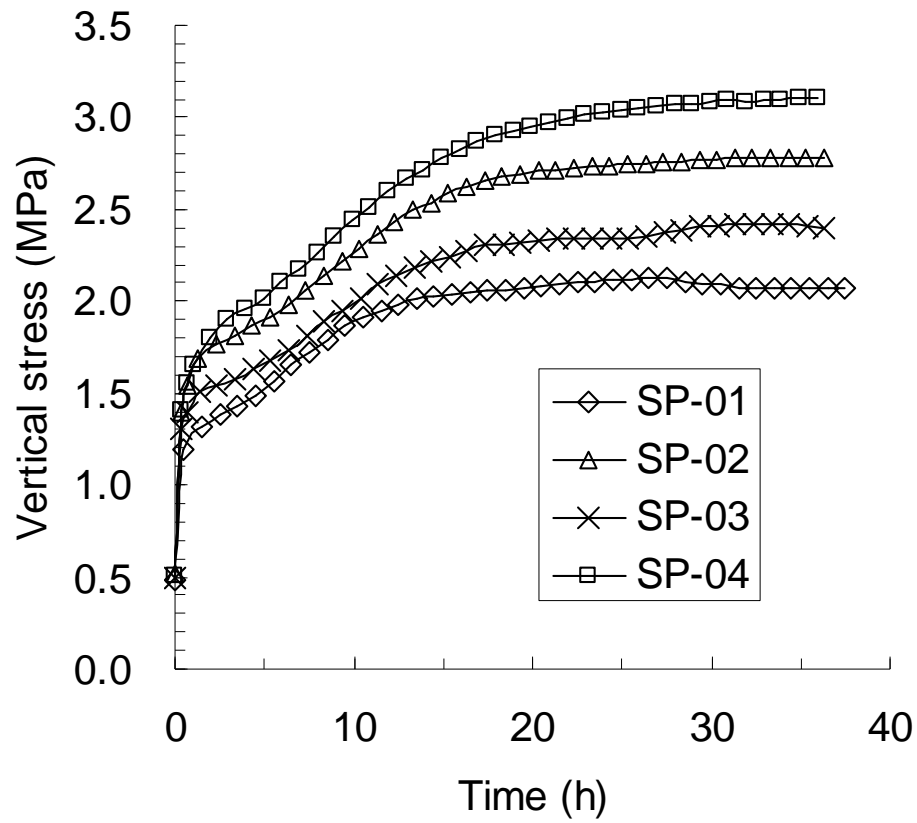
796
797 Figure 9. Evolution of the vertical stress for all hydration tests with technological void
798
799
800
801
802
803
804
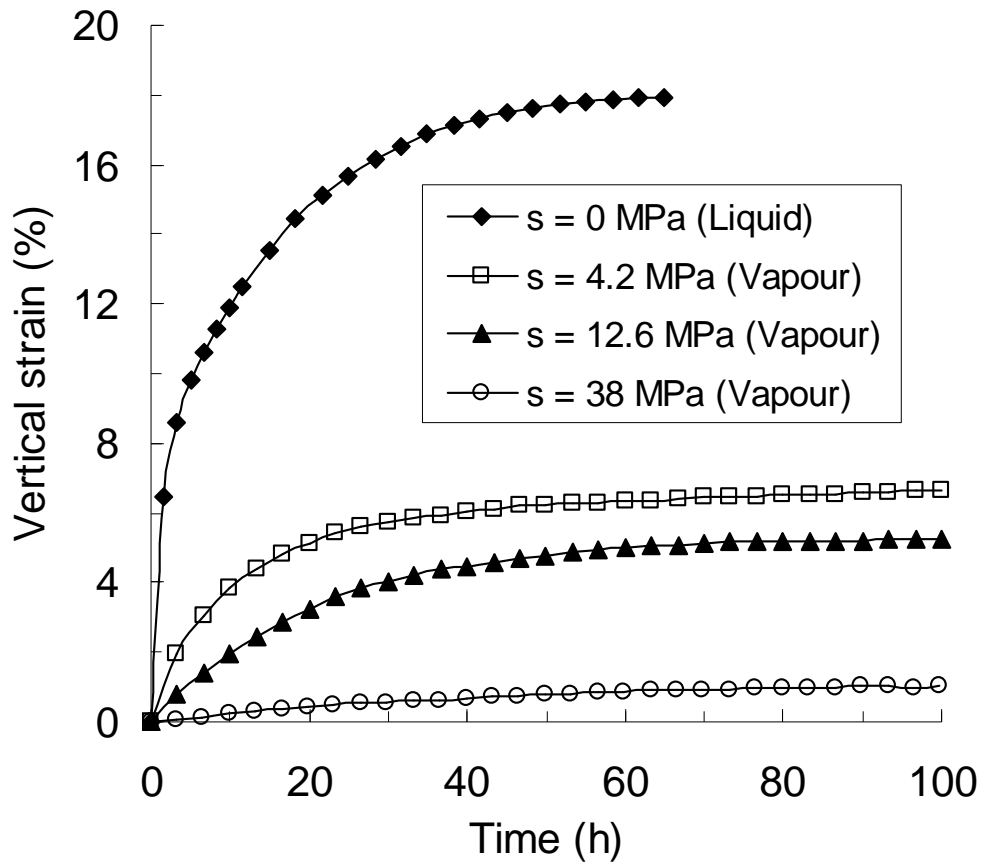
805
806   Figure 10. Evolution of vertical strain during suction imposition
807
808
809
810
811
812
813
814
815
816

817
818 Figure 11. Relationship between void ratio and suction for the compacted sand bentonite
819 mixture.
820
821

822

823 Figure 12. Void ratio of soil versus vertical net stress for different suctions

824

825

826

827
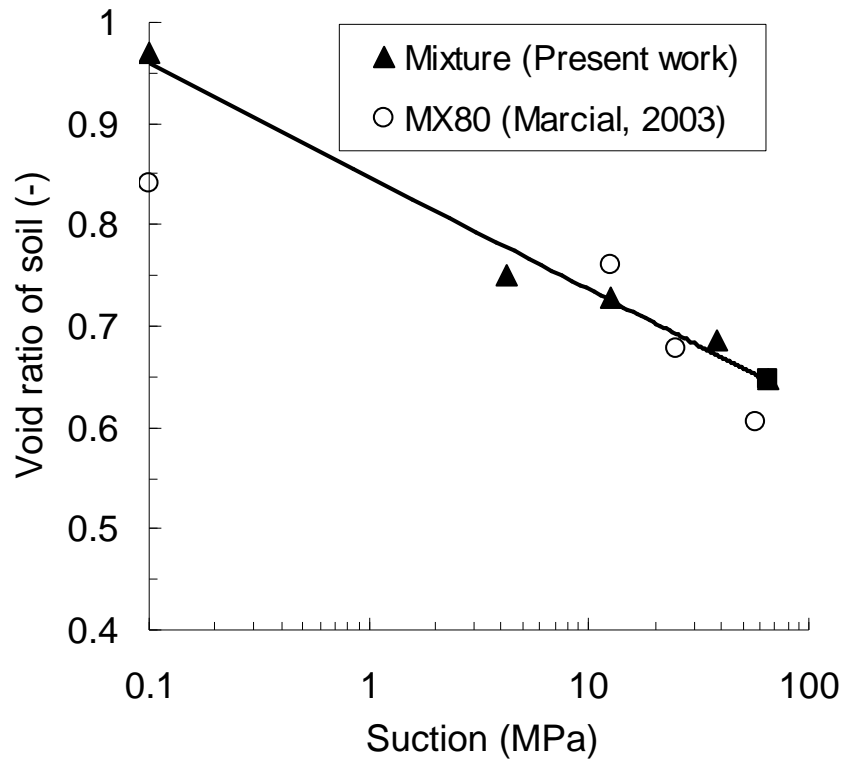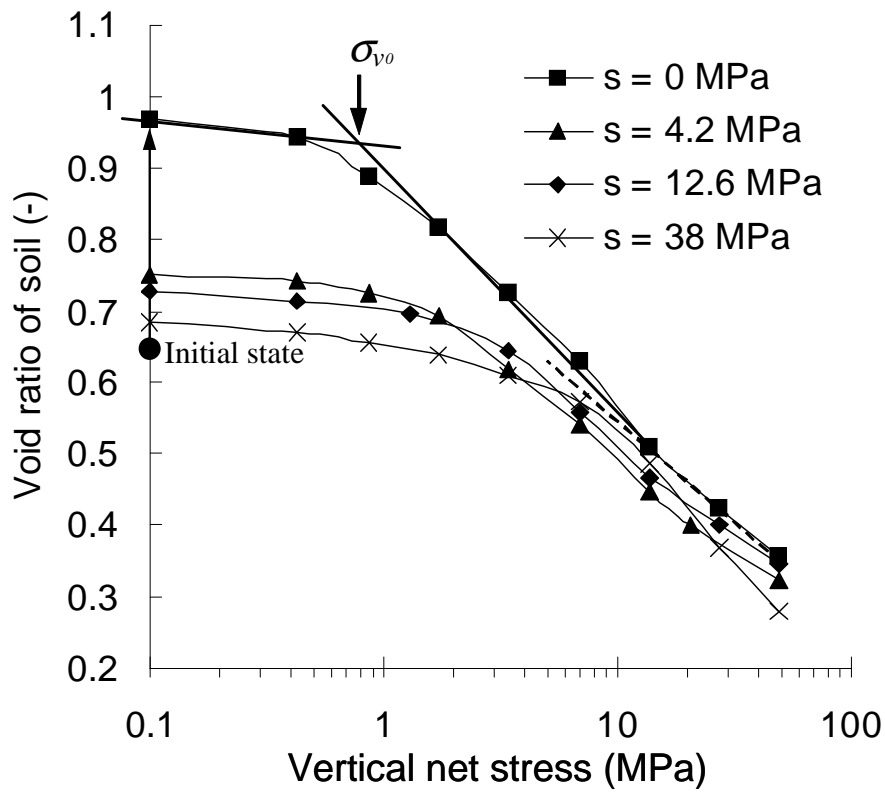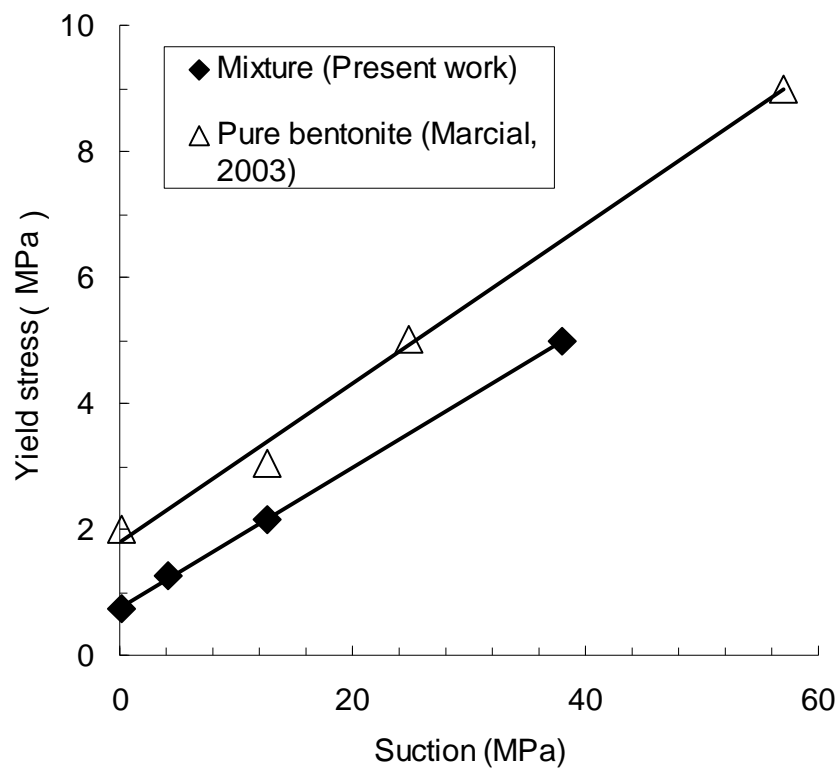
828   Figure 13. Changes in yield stress with suction

829
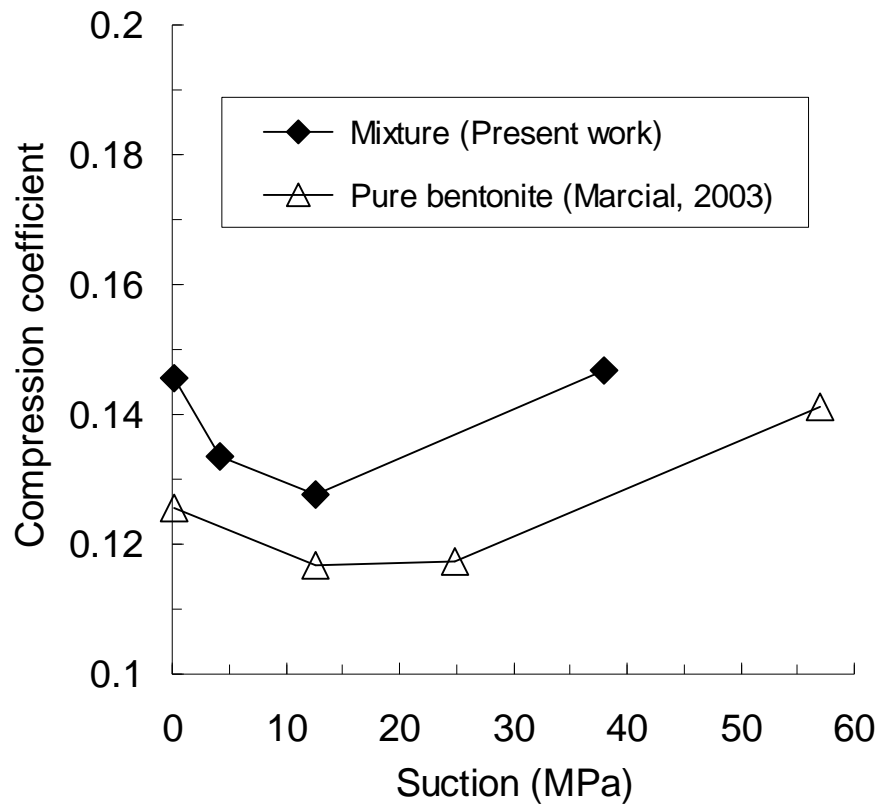
830

831   Figure 14. Changes in compression coefficient with suction
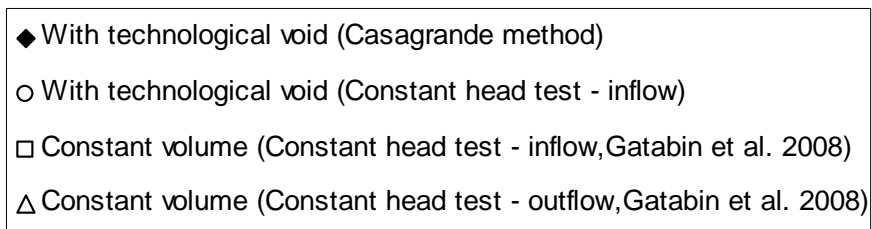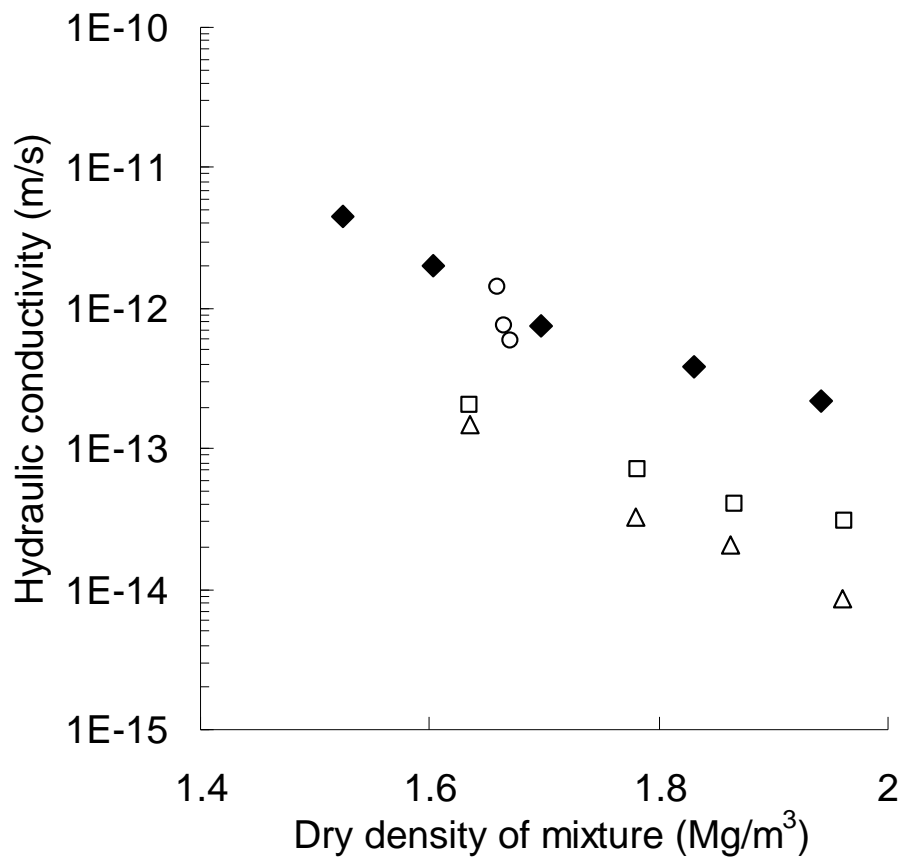
832

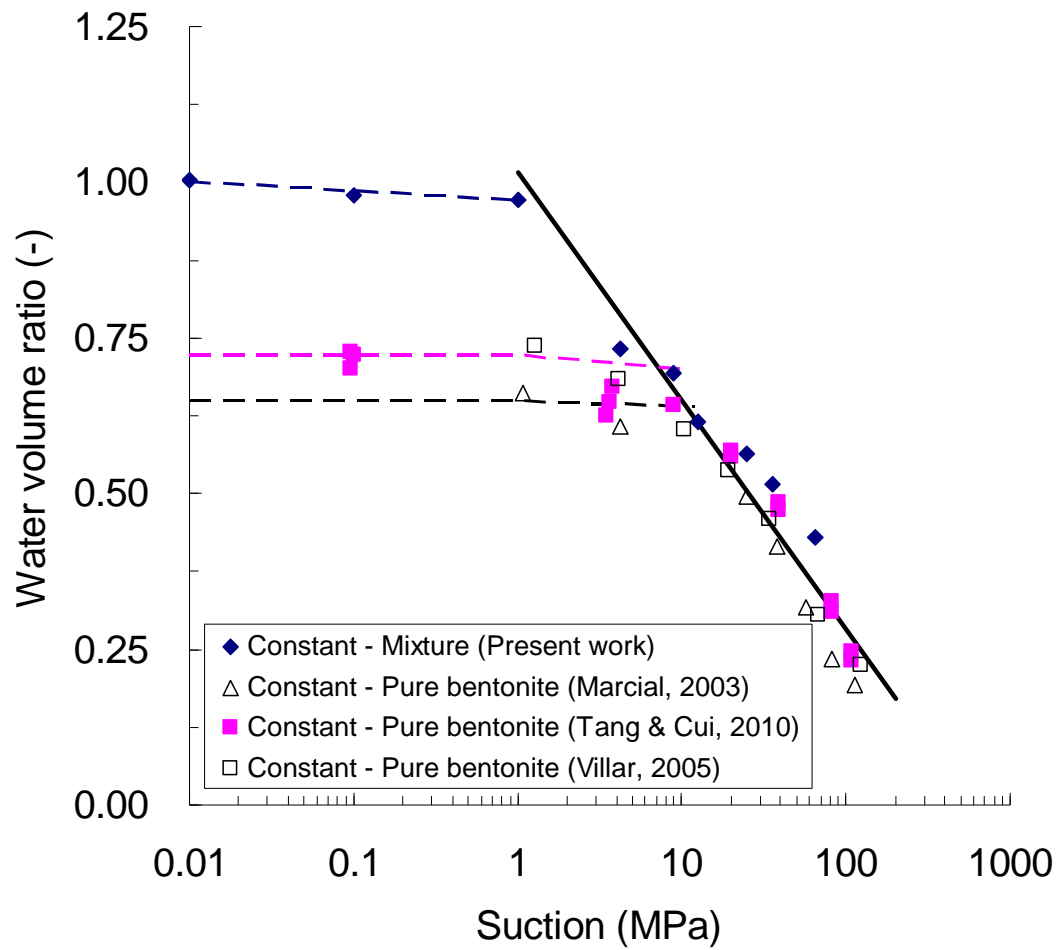833   Figure 15. Hydraulic conductivity versus dry density of mixture

834

835

836
837 Figure 16. Composition of the bentonite/sand mixture
838
839
840
841
842
843

844

845

846

847 (a)

848

849
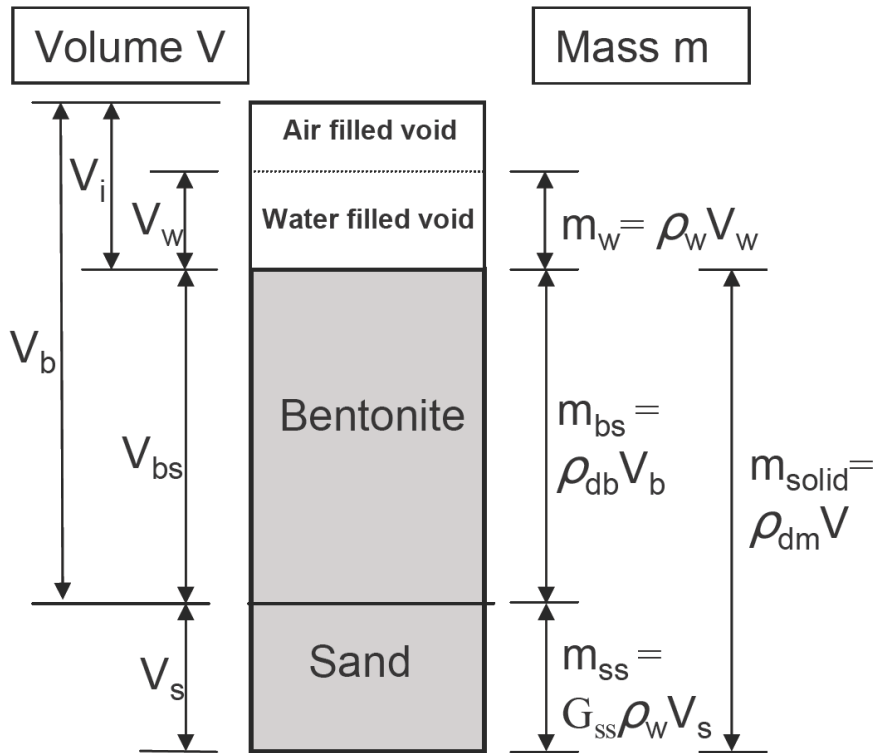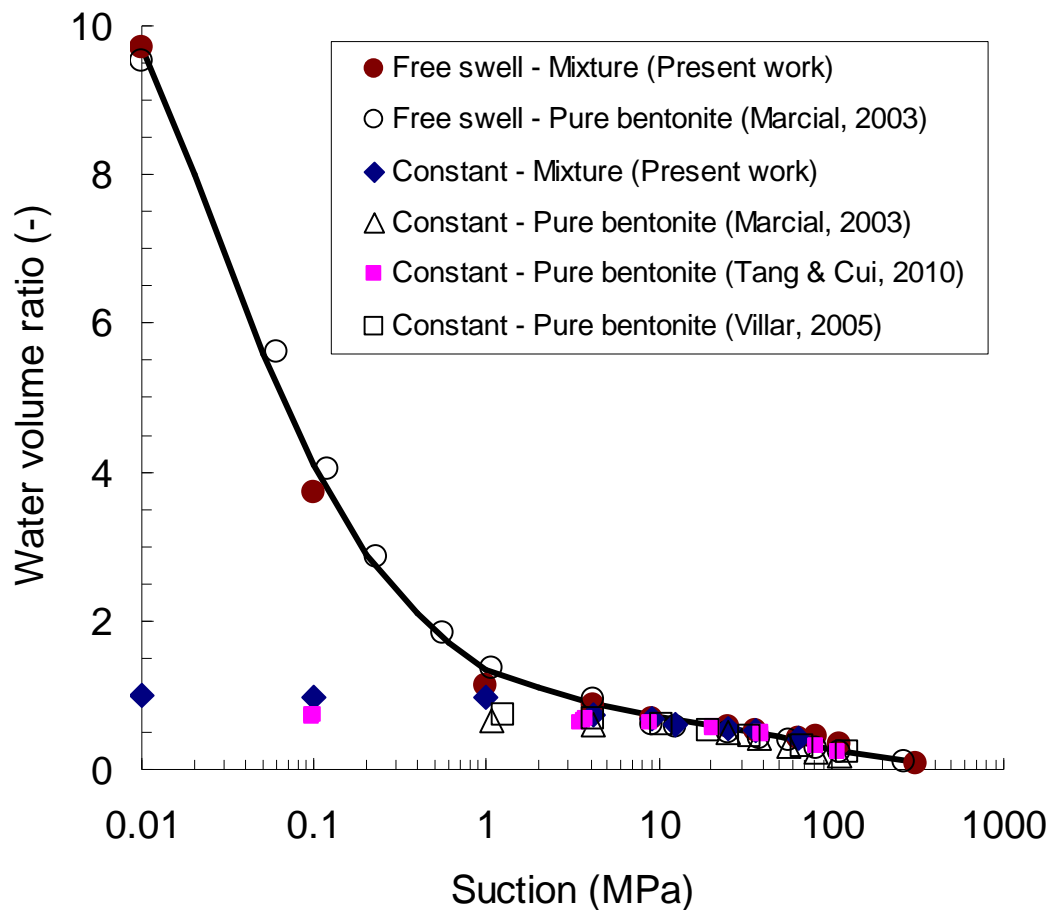
850     $\rho_{db} = 1.70$ Mg/m^3 (Marcial, 2003);

851     $\rho_{db} = 1.60$ Mg/m^3 (Tang et al., 2010; Villar, 2005);

852     $\rho_{db} = 1.43$ Mg/m^3 (Present work);

853   b)

854 Figure 17. Water volume ratio (e_w) Versus suction. a) full range of water volume ratio; b)

855 zoom on the range of low water volume ratio

856

857

858

859

860

861

862

863

864
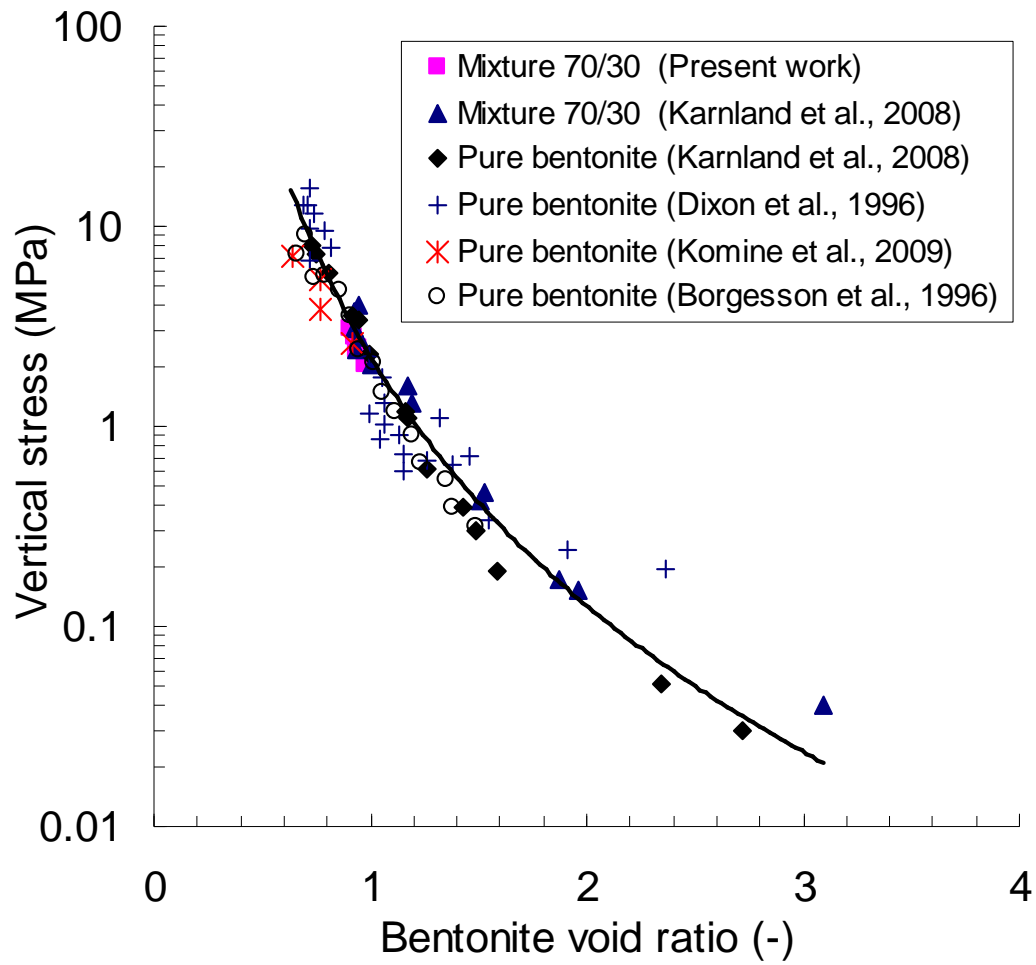
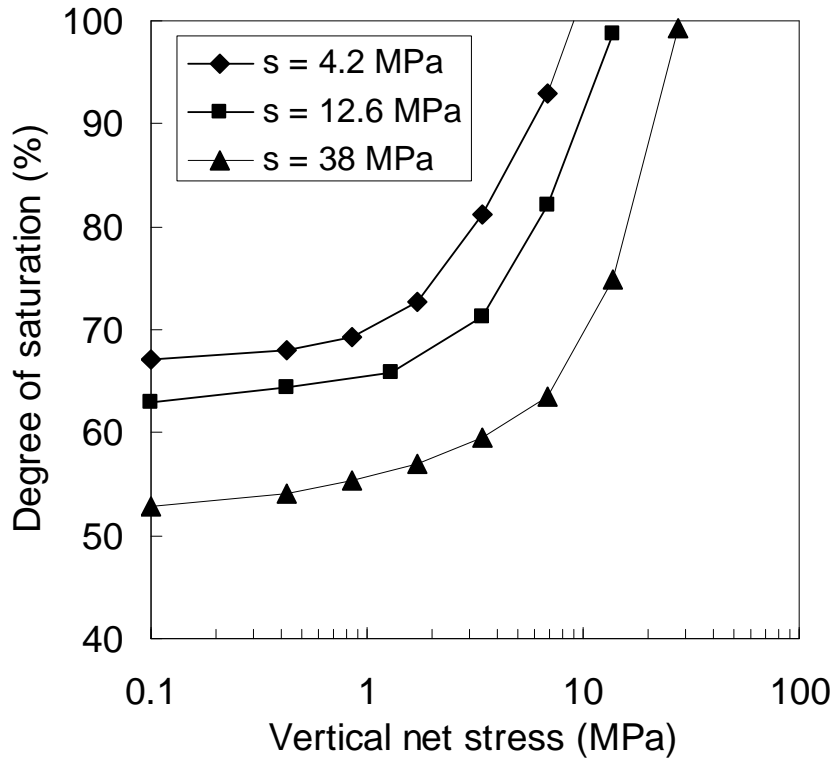Figure 18. Relationship between vertical stress and bentonite (MX 80) void ratio

872

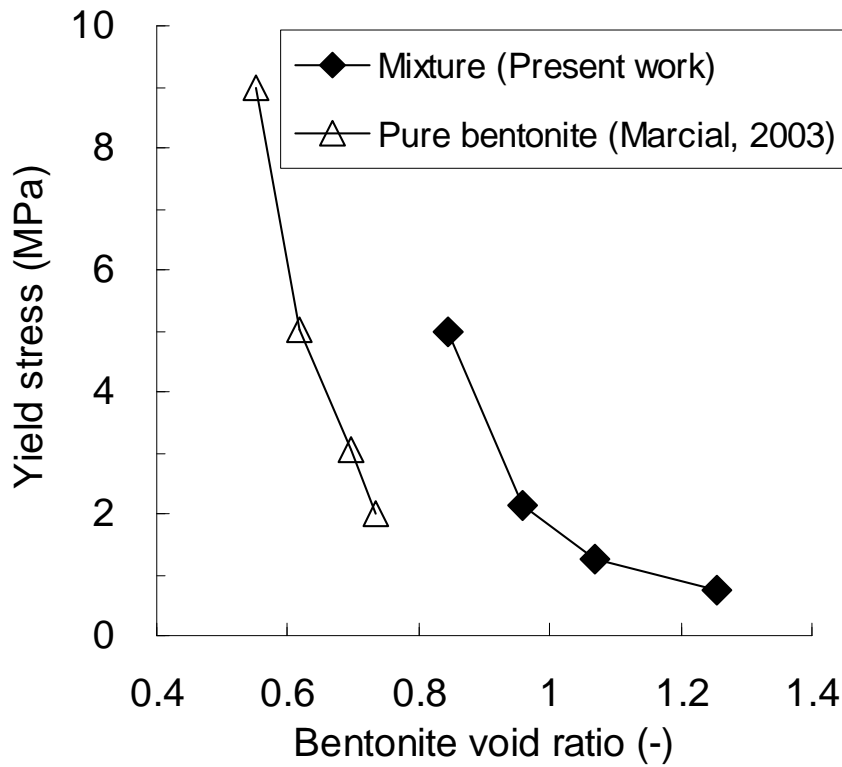Figure 19.   Changes in degree of saturation during compression

874

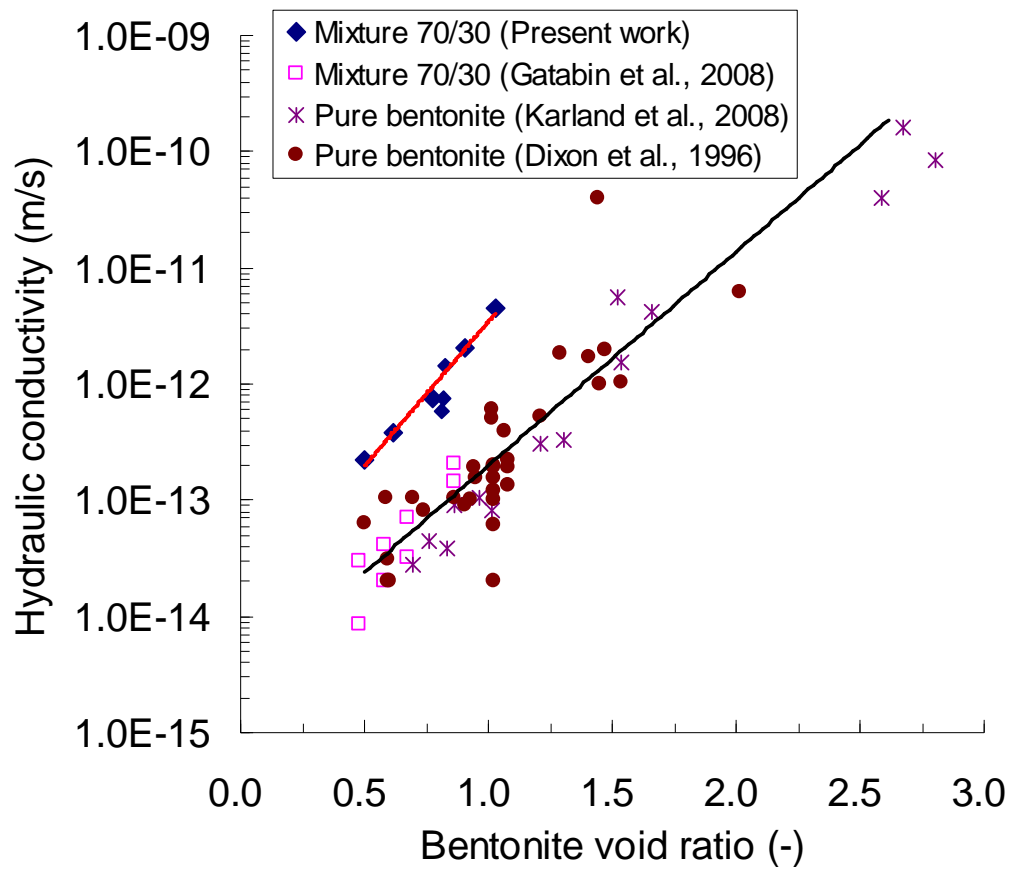Figure 20. Relationship between yield stress and bentonite void ratio

876

877

878 Figure 21. Hydraulic conductivity versus bentonite void ratio

879

880 Photo 1. Water outflow through the technological void.

881